bioRxiv preprint doi: https://doi.org/10.1101/527267; this version posted January 22, 2019. The copyright holder for this preprint (which was not certified by peer review) is the author/funder, who has granted bioRxiv a license to display the preprint in perpetuity. It is made available under aCC-BY 4.0 International license.

The biofilm matrix scaffold of *Pseudomonas* species consists of non-canonically base paired extracellular DNA and RNA

Thomas Seviour[1,*], Fernaldo Richtia Winnerdy[2], Lan Li Wong[1], Xiangyan Shi[2], Sudarsan Mugunthan[1], Gurjeet Singh Kohli[1], Heather M Shewan[3], Jason R Stokes[3], Scott A Rice[1,4,5], Anh Tuân Phan[2], Staffan Kjelleberg[1, 5, 6]

[1] Singapore Centre for Environmental Life Sciences Engineering, Nanyang Technological University, 637551, Singapore.

[2] School of Physical and Mathematical Sciences, Nanyang Technological University, 637371, Singapore.

[3] School of Chemical Engineering, The University of Queensland, 4072, Brisbane, Australia.

[4] The iThree Institute, The University of Technology Sydney, Sydney, 2007, Australia.

[5] School of Biological Sciences, Nanyang Technological University, 637551, Singapore.

[6] Centre for Marine Bio-Innovation, School of Biological, Earth and Environmental Sciences, University of New South Wales, Sydney, 2052, Australia.

*Correspondence to: twseviour@ntu.edu.sg

bioRxiv preprint doi: https://doi.org/10.1101/527267; this version posted January 22, 2019. The copyright holder for this preprint (which was not certified by peer review) is the author/funder, who has granted bioRxiv a license to display the preprint in perpetuity. It is made available under aCC-BY 4.0 International license.

Abstract

While the array of emergent properties assigned to biofilms is extensive (e.g. antimicrobial tolerance), the mechanisms that underpin these are largely unknown. In particular, the extracellular matrix, a defining feature of biofilms, remains poorly understood in terms of its composition and contribution to biofilm structure and function. Here we demonstrate that extracellular DNA exists in a complex with RNA that forms the main cross-linking exopolymer of *Pseudomonas* biofilms, and explains biofilm elasticity. The RNA has a high purine content and our solid-state NMR data indicate the formation of Hoogsteen guanine base pairs. This may suggest the presence of G-quadruplexes, which is also corroborated by the enhancement of biofilm formation in the presence of potassium. The finding that non-canonical interactions mediate networking of matrix-forming extracellular nucleic acids addresses how eDNA is organized and contributes to matrix biophysical properties. This understanding will allow for the development of more effective biofilm control strategies.

bioRxiv preprint doi: https://doi.org/10.1101/527267; this version posted January 22, 2019. The copyright holder for this preprint (which was not certified by peer review) is the author/funder, who has granted bioRxiv a license to display the preprint in perpetuity. It is made available under aCC-BY 4.0 International license.

Introduction

Biofilms are key microbial ecosystems that contribute to bacterial pathogenicity (Phillips and Schultz, 2012), disrupt flow in water filtration systems (Drescher et al., 2013) and facilitate wastewater treatment bioprocesses (Seviour et al., 2011). They represent bacterial adaptation strategies allowing for increased antibiotic tolerance (Høiby et al., 2010), enhanced resource capture (Kurniawan et al., 2012) and the establishment of ecological microniches (de Kreuk et al., 2007). Such properties are unique to biofilms, in contrast to planktonic bacteria, and are not mediated directly by the cells but instead by an extracellular polymeric matrix the cells secrete (Flemming and Wingender, 2010).

Exopolymer functions in biofilms have been studied extensively (Seviour et al., 2012), particularly for *Pseudomonas aeruginosa*, which contributes to one in five clinical infections (Bodey et al., 1983). No fewer than eight exopolymers have been identified as supporting key traits in *P. aeruginosa* biofilms, including three exopolysaccharides (Colvin et al., 2012), four proteins (Allesen-Holm et al., 2006; Borlee et al., 2010; Seviour et al., 2015a) and extracellular DNA (eDNA) (Okshevsky and Meyer, 2015). Each putative exopolysaccharide (Colvin et al., 2012) has been identified as a primary structural agent, suggesting the existence of functional redundancy. Other exopolymers have multiple roles (Irie et al., 2012) and a wide range of secondary regulatory responses associated with *P. aeruginosa* biofilm exopolymer expression has been elucidated (Herbst et al., 2015).

Despite the ambiguity of the contributions of individual exopolymers, biofilm formation is the result of these exopolymers changing the matrix's viscous and elastic properties (i.e. viscoelasticity), where viscosity refers to its fluid properties and elasticity its networked properties. Polymeric networking is a fundamental requirement for any biofilm (Chew et al.,

bioRxiv preprint doi: https://doi.org/10.1101/527267; this version posted January 22, 2019. The copyright holder for this preprint (which was not certified by peer review) is the author/funder, who has granted bioRxiv a license to display the preprint in perpetuity. It is made available under aCC-BY 4.0 International license.

2014). We undertook to identify the foundation polymer/s in *P. aeruginosa* biofilms, which are defined here as those that either dominate biofilm elasticity or constitute the primary structural agent/s.

Results

eDNA dominates the elastic response of *Pseudomonas aeruginosa.*

To characterize the foundation polymer of *P. aeruginosa* biofilms we exploited the reported ability of the ionic liquid 1-ethyl-3-methyl-imidazolium acetate (EMIM-Ac) to dissolve a range of recalcitrant biopolymers, including DNA(Zhao, 2015) and cellulose (Vitz et al., 2009), which led us to demonstrate this also for *P. aeruginosa* biofilm exopolymers (Seviour et al., 2015b). Here, when *P. aeruginosa* biofilms were dissolved in EMIM-Ac, the subsequent fluid was highly viscoelastic. We measured non-linear elasticity as a shear-rate dependent high normal stress difference (N_1-N_2), where N_1 and N_2 are primary and secondary normal stress differences respectively. Elasticity dominated the viscous flow properties for the wild type biofilm in EMIM-Ac, with (N_1-N_2) an order of magnitude greater than shear stress (Figure 1A; Wild type). The solvent (EMIM-Ac) alone exhibited no elasticity, indicating that the elastic properties are transferred to the EMIM-Ac from the biofilm matrix. Viscosity was slightly shear-thinning (Supplementary Figure 1A and Supplementary Table 1), which would be expected from dilute polymer solutions in viscous fluids (i.e. Boger fluids) (Scirocco et al., 2005). (N_1-N_2), has a power law dependence on the shear rate (n) of 1.4 (Supplementary Figure 1B, Wild type) and viscoelasticity was accurately modeled by the modified, finitely-extensible nonlinear elastic (FENE-P) polymer model (Figure 1A-B; Supplementary Tables 1 and 2). The rheological

bioRxiv preprint doi: https://doi.org/10.1101/527267; this version posted January 22, 2019. The copyright holder for this preprint (which was not certified by peer review) is the author/funder, who has granted bioRxiv a license to display the preprint in perpetuity. It is made available under aCC-BY 4.0 International license.

behavior is thus characteristic of solutions containing semi-flexible polymers, such as DNA(Stokes et al., 2001).

The polysaccharides alginate, Pel and Psl have been suggested as the structural scaffolds of *P. aeruginosa* biofilms (Colvin et al., 2012). Their contribution to elasticity was determined using the mucoid, alginate over-expressing strain PDO300 and isogenic Pel and Psl genetic knockout mutants (Ghafoor et al., 2011). When Psl is absent, the elasticity (i.e. N_1-N_2) and viscosity increased relative to the wild type and the mucoid strain PDO300, which was less elastic than the wild type despite the over-expression of alginate (Figure 1; ΔPsl). In contrast, when Pel is absent, there was a slight decrease in both elasticity and viscosity relative to both the wild type and PDO300 (Figure 1; ΔPel).

The contributions of proteins, RNA and DNA were also explored using pronase, RNase A and DNase I, respectively (Figure 1; Pronase, RNase, DNase). Removing each exopolymer component individually decreased biofilm elasticity. With the exception of the DNase I-treated biofilm, all treatments displayed *n* values of 0.9 – 1.7 (Supplementary Table 1), consistent with semi-flexible polymers like DNA(Mansfield et al., 2015). While viscosity was unchanged following pronase treatment, there was a slight decrease in elasticity. This decrease in elasticity was even greater following RNase treatment, and elasticity was completely lost upon DNase treatment, with the normal stress difference reduced to zero. Thus, the elastic response of the biofilm in EMIM-Ac can be primarily attributed to DNA.

The fundamental rheology described here for the *P. aeruginosa* biofilm therefore arises principally from DNA. This was elucidated for biofilms dissolved in EMIM-Ac as well as for hydrated, native biofilms displaying the same structural dependence on DNA (Supplementary Figure 2). This approach of dissolving biofilm in EMIM-Ac to assess the contribution of

bioRxiv preprint doi: https://doi.org/10.1101/527267; this version posted January 22, 2019. The copyright holder for this preprint (which was not certified by peer review) is the author/funder, who has granted bioRxiv a license to display the preprint in perpetuity. It is made available under aCC-BY 4.0 International license.

individual exopolymers to its properties is thus validated. The data suggest that multiple exopolymers contribute to the rheology, with the matrix from the ΔPsl mutant being the most elastic, followed by wild type and RNase A-treated biofilms, which were the least elastic. It has been noted previously that a range of *P. aeruginosa* exopolymers influence biofilm extracellular matrix crosslinking (Colvin et al., 2012), and the data presented further clarifies that these exopolymers can only modulate biofilm rheology if eDNA is present. An eDNA scaffold is therefore a prerequisite for this rheological differentiation of the matrix. Further support for the presence of an eDNA scaffold is provided in the micrograph of a biofilm stained with TOTO-1 for DNA visualization (Figure 1C), which shows DNA fibers in the extracellular matrix.

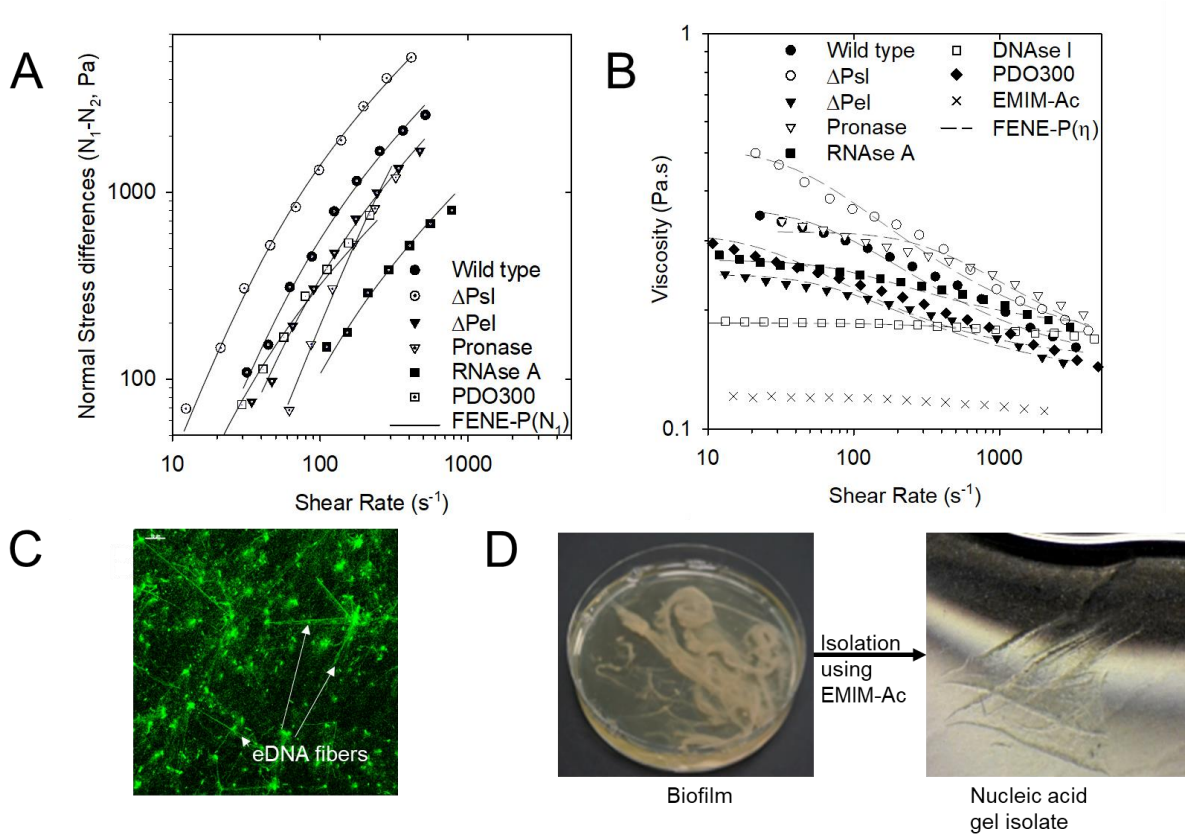

Figure 1: (A) N_1-N_2 and (B) viscosity against shear rate for *Pseudomonas aeruginosa* biofilm wild type, PDO300, ΔPsl, ΔPel, and pronase, RNase A and DNase I digested wild type biofilm immediately following dissolution in 1-ethyl-3-methylimidazolium acetate (40 mg/mL) at 25 °C, 100 µm gap. This is measured as a function of shear stress

bioRxiv preprint doi: https://doi.org/10.1101/527267; this version posted January 22, 2019. The copyright holder for this preprint (which was not certified by peer review) is the author/funder, who has granted bioRxiv a license to display the preprint in perpetuity. It is made available under aCC-BY 4.0 International license.

from 10 to 1000 Pa. ($N_1 - N_2$) is not described for DNase I digested biofilm in Figure 1A and Supplementary Figure 1B as their normal force (F_N) is less than the resolution of the rheometer (i.e. 0.1 N) and set to zero for calculating ($N_1 - N_2$). Both the N_1-N_2 and viscosity data are fitted with the FENE-P model, a rigid dumbell model for polymer solutions. Fitting parameters are shown in Supplementary Table 2. (C) Micrograph of *P. aeruginosa* biofilm DNA stained green with TOTO-1 (scale bar 10 μm). (D) Phase separation of extracellular nucleic acids extracted from *P. aeruginosa* biofilms into a gel occurs upon transfer from 1-ethyl-3-methylimidazolium acetate into water.

Furthermore, EMIM-Ac did not lyse either biofilm or planktonic cells as indicated by the intact cell morphology and the absence of phospholipids and lipopolysaccharides in EMIM-Ac following biofilm dissolution (Supplementary Figure 3). Therefore, it was concluded that the DNA dissolved following treatment of *P. aeruginosa* planktonic cells and biofilms with EMIM-Ac is extracellular and due to extraction of intracellular DNA.

This finding that eDNA is a prerequisite for matrix building is consistent with recent studies reporting the observation of eDNA in biofilm extracellular matrices (Jennings et al., 2015). That DNA dominated the elastic response would indicate eDNA is not an incidental matrix component but instead a primary, or foundation structural component of *P. aeruginosa* biofilms.

Isolated nucleic acids mimic gel-forming property of *P. aeruginosa* biofilms.

eDNA is known to complex and co-localize with exopolysaccharides. Furthermore, eDNA sequencing shows that there is no bias towards any specific region of the chromosome (Turnbull et al., 2016). In contrast to intracellular chromosomal DNA, which is supercoiled and folded, for example, by HU proteins and topoisomerases, and then relaxed by gyrases to allow replication and transcription to occur, the organization of eDNA remains elusive. We contend that a molecular understanding of how the eDNA is assembled and organized is key to answering how and why DNA transforms from the chromosomal form to that found in the biofilm matrix.

bioRxiv preprint doi: https://doi.org/10.1101/527267; this version posted January 22, 2019. The copyright holder for this preprint (which was not certified by peer review) is the author/funder, who has granted bioRxiv a license to display the preprint in perpetuity. It is made available under aCC-BY 4.0 International license.

We recovered the eDNA from EMIM-Ac following biofilm dissolution by exploiting the ability of perchloric acid to selectively precipitate DNA over protein (Supplementary Figure 4). Following further purification by gel permeation chromatography, the polymer phase-separated into a gel upon transfer from EMIM-Ac into water (i.e. the gel isolate), mimicking the formation of networks in native biofilms (Figure 1D). A higher *G'* was recorded for the gel isolate than for the *P. aeruginosa* biofilm (Supplementary Figure 5), which is consistent with it having a higher DNA concentration. Furthermore, DNase degraded the isolated gel into shorter DNA fragments (Supplementary Figure 6). Other fractions, including those not precipitated by perchloric acid, did not self-assemble into gels (Supplementary Figure 7A). Similarly, calf thymus DNA did not form gels when processed the same way, either with or without added cations (Supplementary Figure 7B), suggesting that this behavior is not a universal property of DNA.

Nucleic acid conformation is preserved during isolation.

Circular dichroism (CD) is an extremely sensitive spectroscopic technique for determining the secondary structure of biomolecules, particularly proteins and nucleic acids. It was used here to understand whether the nucleic acid (NA) conformation was modified during extraction and isolation. Unprocessed *P. aeruginosa* biofilms displayed a major circular dichroism (CD) peak at 250-285 nm (Figure 2A), which is consistent with the presence of NA (Kypr et al., 2009) and this peak was also observed to dominate the CD spectrum of the gel isolate (Figure 2B). The spectral trough at 225.5-226.5 nm is typical for proteins (Greenfield, 2006). NA can also display a trough in this region, although the relative depth of the trough and its absence after proteolysis and fractional precipitation against proteins (Supplementary Figure 4) suggest that it denotes proteinaceous material. Hence, even though the CD spectrum shows that proteins are significant

bioRxiv preprint doi: https://doi.org/10.1101/527267; this version posted January 22, 2019. The copyright holder for this preprint (which was not certified by peer review) is the author/funder, who has granted bioRxiv a license to display the preprint in perpetuity. It is made available under aCC-BY 4.0 International license.

components of the biofilm matrix, they are not major contributors to biofilm elasticity (Figure 1A).

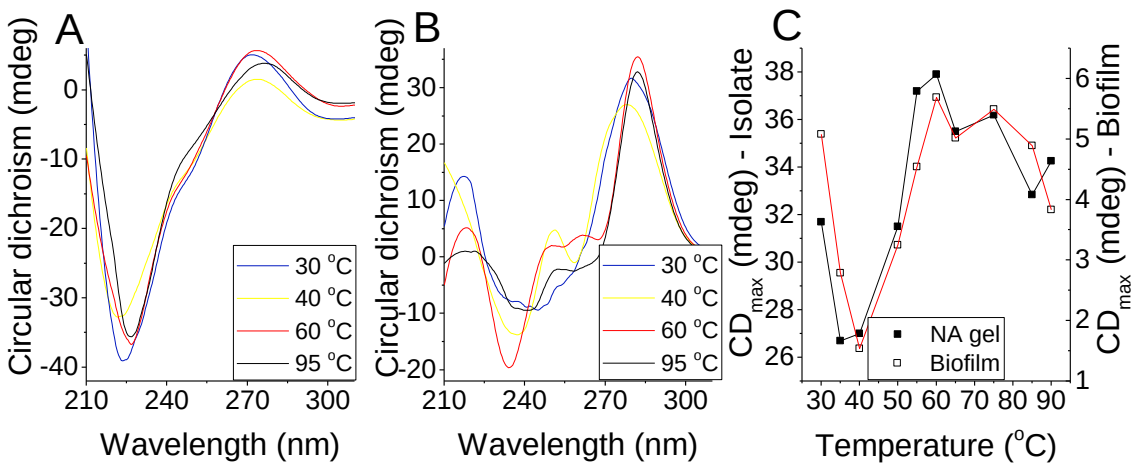

Figure 2: Circular dichroism (CD) spectra of (A) *Pseudomonas aeruginosa* biofilm and (B) extracellular nucleic acids (NA) gel isolate at temperatures between 30 and 95°C. (C) Amplitude of dominant NA peak, CD_{max} (260-285 nm), from CD spectra of *P. aeruginosa* biofilm (seen in (A)) and its extracted extracellular nucleic acid gel (seen in (B)) from T = 30°C to T = 95°C.

The CD spectrum of the isolated NA gel (Figure 2B) is dominated by the same NA peak that appears in the biofilm CD spectrum. To confirm this similarity, CD melting experiments were performed on both samples. The resulting melting curves (Figure 2C) show that their maximum absorbance values follow the same trend across the temperature profiles, with a minimum absorbance at 40°C, a maximum at 60°C and only partial absorbance attenuation at 95°C. NA conformation was thus preserved during its isolation and the NA are more stable than typical, canonical DNA duplexes (Khandelwal and Bhyravabhotla, 2010). The extracted NA gel isolate is therefore an accurate proxy for understanding the intermolecular interactions that stabilize the extracellular matrices of *P. aeruginosa* biofilms. Moreover, the CD spectrum of the NA gel isolate informs on the nucleic acid conformation. In addition to the peak at 272 nm, there is a trough that shifts from 245 to 230 nm with increasing temperature, another maximum at 215 nm

bioRxiv preprint doi: https://doi.org/10.1101/527267; this version posted January 22, 2019. The copyright holder for this preprint (which was not certified by peer review) is the author/funder, who has granted bioRxiv a license to display the preprint in perpetuity. It is made available under aCC-BY 4.0 International license.

that remains constant with temperature, and other sub-maxima at 260 and 253 nm that change with temperature. The absence of a trough at 200-215 nm precludes the possibility of NA in A- or Z- conformations (Kypr et al., 2009). The dominant maximum and minimum could indicate either B-DNA or G-quadruplex conformations (del Villar-Guerra et al., 2018), although the peak at 215 nm is not a feature of B-DNA CD spectra and is slightly higher than the characteristic G-quadruplex low wavelength peak of 210 nm. Nonetheless, the appearance of several peaks in the NA region of 250-285 nm indicates that, while the dominant NA conformation is unclear, several conformations likely contribute to phase separation of the NA.

Purine-rich ribonucleotides and eDNA are present in isolated gel.

Total correlation spectroscopy (TOCSY) and ^{1}H-^{13}C heteronuclear single quantum coherence (HSQC) are nuclear magnetic resonance (NMR) techniques that can identify proton NMR correlations within individual ribose sugars and their proton-carbon single bond correlations respectively. Raising the pH can solubilize *P. aeruginosa* biofilms (Friedman and Kolter, 2004) and here we show that after alkalinization, the NA peaks dominated the solution ^{1}H-^{13}C HSQC spectra for the isolated material with no indication that proteins or polysaccharides were present (Supplementary Figure 8; (Wüthrich, 2008)). The ^{1}H-^{13}C HSQC-TOCSY spectrum of the isolated gel when dissolved by alkalinization shows two clusters of sugar proton peaks (C1'-H1') with correlations to neighboring carbons (C2'-H1') (Figure 3A).

The first cluster (rectangles) has C2' chemical shift values of ~40 ppm and the second cluster (ovals) has C2' values of ~70 ppm. The ^{1}H-^{13}C correlations denoted by the rectangles therefore arise from deoxyribose and those denoted by the ovals from ribose sugar conformations. The broadened form of the deoxyribonucleotide peaks is consistent with high molecular weight (MW) molecules, while the sharpness of the ribonucleotide peaks suggests that they could arise

bioRxiv preprint doi: https://doi.org/10.1101/527267; this version posted January 22, 2019. The copyright holder for this preprint (which was not certified by peer review) is the author/funder, who has granted bioRxiv a license to display the preprint in perpetuity. It is made available under aCC-BY 4.0 International license.

from small, possibly even single nucleotides. Hence, eDNA and small ribonucleotides are both likely to be present in the gel dissolved by alkalinization.

Spin-systems for the eight sharp ribonucleotide peaks (Figure 3B) were assigned by HSQC-TOCSY and correlation spectroscopy (COSY) (Supplementary Figure 9) with absolute identification achieved by comparing the heteronuclear multiple bond correlation HMBC spectra of samples and monoribonucleotide standards (Supplementary Figure 10). The ^{31}P NMR spectrum of the NA gel isolate at elevated pH revealed the presence of a mixture of monoesterified (3.4 to 4.1 ppm) and diesterified phosphates (-0.8 to -1.2 ppm), indicating the coexistence of monoribonucleotides and DNA respectively (Figure 3C (i)). Long-range ^{31}P-^{1}H correlations (i.e. from NA phosphorous to adjoined ribose proton) were observed in the ^{31}P-^{1}H heteronuclear correlation (HETCOR) spectrum (Figure 3C (ii)) for both monoribonucleotides and DNA. The broad ^{31}P-^{1}H cross peaks at ~-1.0 ppm (Figure 3C (ii)) correspond to long-range correlations between DNA phosphorous to H3’ and H5’/H5’’ protons. The eight monoribonucleotides were assigned to 2’- and 3’-(A, U, G, and C)-monophosphates. We therefore have both 2’ and 3’ monoribonucleotides present with the eDNA in the gel solubilized under alkaline conditions.

However, the monoribonucleotide peaks only became resolved upon alkaline dissolution of the biofilm, in contrast to the broad peaks evident at pH 7 (Supplementary Figure 11). This indicates that the monoribonucleotides are derived from chain structures that exist at biological pH and assemble with DNA chains into higher-order networked structures, which is consistent with the observation in Figure 1A that RNA is a major contributor to *P. aeruginosa* biofilm elasticity.

bioRxiv preprint doi: https://doi.org/10.1101/527267; this version posted January 22, 2019. The copyright holder for this preprint (which was not certified by peer review) is the author/funder, who has granted bioRxiv a license to display the preprint in perpetuity. It is made available under aCC-BY 4.0 International license.

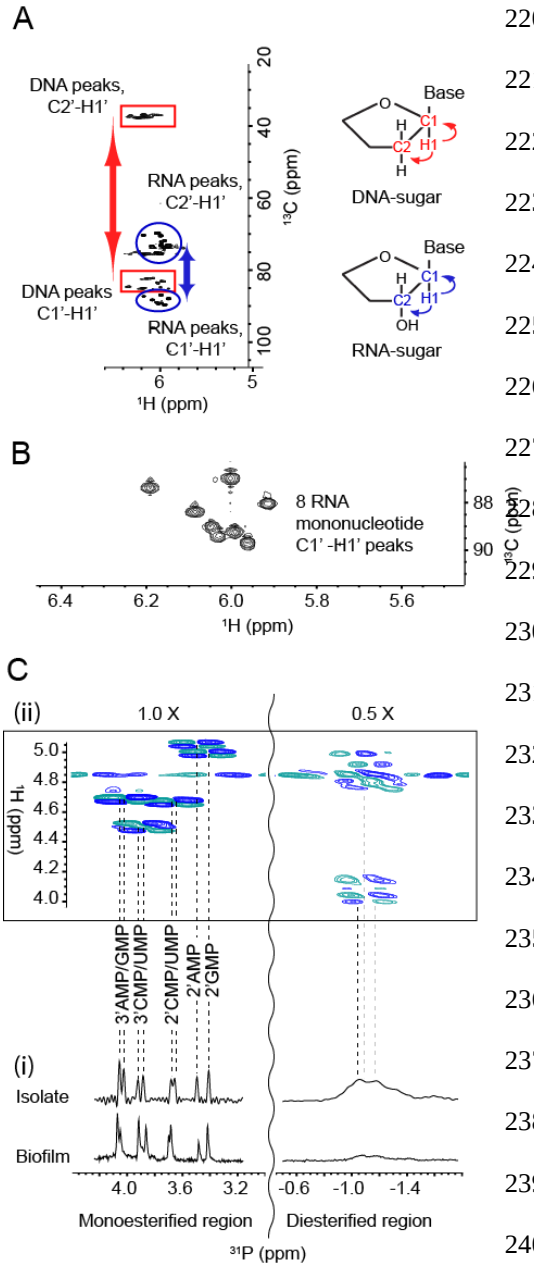

Figure 3: (A) Nuclear magnetic resonance (NMR) ^{1}H-^{13}C heteronuclear single quantum coherence (HSQC)-total correlation spectroscopy (TOCSY) spectrum at 25°C of extracellular nucleic acids (NA) gel isolate after alkalinization showing the C1'-H1' cross peaks of RNA (blue ovals) and DNA (red rectangles) and their correlations to the neighboring carbon C2'-H1'. Schematics (right) illustrate these correlations. (B) ^{1}H-^{13}C HSQC spectrum of extracellular NA gel isolate at 25°C after alkalinization identifying eight monoribonucleic acid ribose spin systems. (C) 1-D ^{31}P NMR of NA isolate gel and *Pseudomomonas aeruginosa* biofilm with proton decoupling showing the presence of monoesterified (i.e. monoribonucleotides) and diesterified (i.e. DNA) phosphate peaks (i), and 2-D ^{1}H-^{31}P heteronuclear correlation (HETCOR) spectrum of extracellular NA showing the ^{31}P-^{1}H cross-peaks of monoribonucleotides and DNA (ii). Couplings of monoesterified phosphates to H2' or H3' of eight monoesterified monoribonucleotides (from left to right: 3' AMP/3' GMP, 3' CMP/3' UMP, 2' CMP/2' UMP, 2' AMP, 2' GMP); and diesterified phosphate to DNA H3' and H5'/H5'' protons, are denoted by the dashed lines. There is a discontinuity (wavy line) in the ^{31}P axis due to the different thresholds required to illustrate the ^{31}P-^{1}H correlations in the mono-esterified and di-esterified regions. All samples were prepared in 0.1 M NaOD (10 mg/mL) and preheated to 55°C for 2 h.

bioRxiv preprint doi: https://doi.org/10.1101/527267; this version posted January 22, 2019. The copyright holder for this preprint (which was not certified by peer review) is the author/funder, who has granted bioRxiv a license to display the preprint in perpetuity. It is made available under aCC-BY 4.0 International license.

The molar ratio of the individual ribonucleotides could be determined from the ^{31}P spectrum of the gel dissolved at high pH (Table 1). While several peaks could not be separated, it was possible to deduce that the RNA is purine rich (i.e. 57 mol% A+G) and that the G+C mol% content of 46-50% differs from that of the *P. aeruginosa* genome (i.e. 67 mol%) (Shen et al., 2006). The same peaks were also observed in the biofilm ^{31}P spectrum after alkalinization (Figure 3C(i)).

Table 1: Relative abundances of monoribonucleotides in extracellular NA gel isolate from *Pseudomonas aeruginosa* biofilm as determined by integrating ^{31}P NMR spectrum following alkalinization.

^{31}P shift (ppm)	Ribonucleotide	Relative abundance
4.03	3'AMP	18.0 %
4.01	3' GMP	17.2 %
3.90	3' CMP/3' UMP	8.9 %
3.87	3' CMP/3' UMP	11.3 %
3.68	2' CMP/2' UMP	9.5 %
3.66	2' CMP/2' UMP	11.7 %
3.50	2' AMP	10.4 %
3.42	2' GMP	13.0 %

Extracellular DNA and RNA interact to form a network.

We applied Magic-angle spinning (MAS) solid-state NMR (SSNMR) to confirm that the networks in the gel isolate and biofilm are comprised of DNA and RNA in chain form. This technique is ideal for intractable systems such as biofilms to eliminate solubility and extraction biases (Reichhardt and Cegelski, 2014), and to analyze inter-molecular H-bond interactions to describe, for example, inter-nucleotide base pairing in RNA (Marchanka et al., 2015). MAS SSNMR averages anisotropic interactions to provide high-resolution spectral characterization of insoluble and large biomolecular systems. By analyzing dipolar interactions, through-space heteronuclear correlations (e.g. N···H) can be detected. In contrast to the liquid state ^{31}P NMR spectrum of the alkali-dissolved isolate (Figure 3C (i)), the ^{31}P SSNMR spectrum of the gel

bioRxiv preprint doi: https://doi.org/10.1101/527267; this version posted January 22, 2019. The copyright holder for this preprint (which was not certified by peer review) is the author/funder, who has granted bioRxiv a license to display the preprint in perpetuity. It is made available under aCC-BY 4.0 International license.

isolate (i.e. no alkali treatment; Figure 4A (i)) showed a single peak in the diesterified phosphate region, consistent with the presence of both DNA and RNA chains. There are no sharp peaks present in the monoesterified phosphate region, further demonstrating that the monoribonucleotides are a consequence of alkali transesterification (Radak et al., 2013).

Only the diesterified phosphate peak was observed in the ^{31}P SSNMR spectrum of the biofilm (Figure 4A (iii)), while both RNA-derived monoesterified and DNA-derived diesterified phosphate peaks were present in the ^{31}P SSNMR spectrum of alkali digested NA gel-isolate and biofilm (lyophilized) (Figure 4A (ii) and Figure 4A (iv), respectively). Complete alkali RNA transesterification was confirmed by the full conversion of diesterified to monoesterified phosphates (from liquid state ^{31}P NMR spectra) for the RNA standard, when dissolved in 0.1 M NaOH (Supplementary Figure 12A). Conversely, RNA diesterified phosphate peaks were preserved in the RNA standard spectrum following dissolution in EMIM-Ac and recovery by perchloric acid (Supplementary Figure 12B). Hence, the alkaline conditions break down the RNA chains into individual monoribonucleotides, while the ionic liquid-based extraction does not. This suggests that the conventional method for *P. aeruginosa* biofilm dissolution in alkali (Friedman and Kolter, 2004) may in fact work by transesterifying RNA as a primary structural component and illustrates the importance of the ionic liquid-based extraction protocol described here as a non-destructive method for interrogating biofilm structural polymers.

bioRxiv preprint doi: https://doi.org/10.1101/527267; this version posted January 22, 2019. The copyright holder for this preprint (which was not certified by peer review) is the author/funder, who has granted bioRxiv a license to display the preprint in perpetuity. It is made available under aCC-BY 4.0 International license.

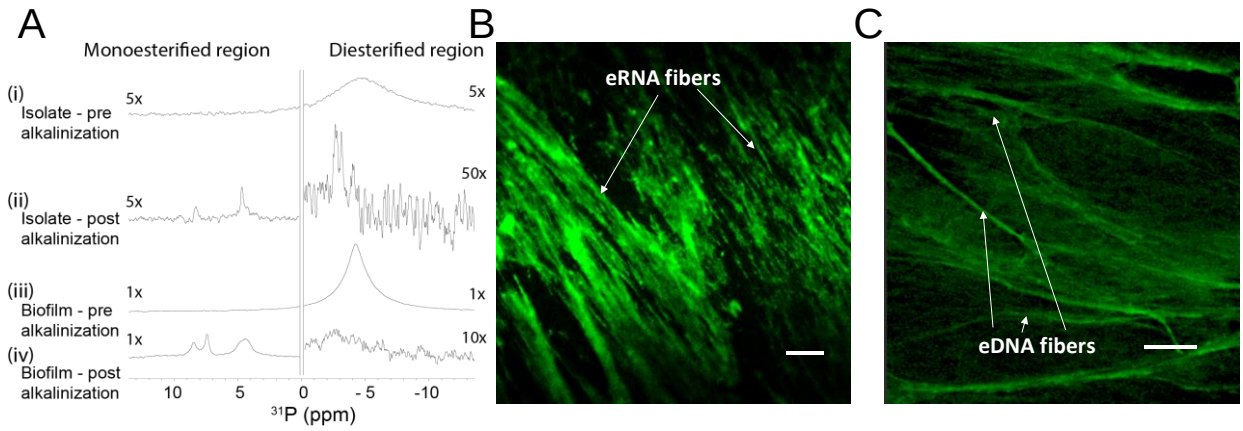

Figure 4: (A) Solid-state ^{31}P NMR spectra at T = 25°C of extracellular NA gel isolate (i), alkalinized and lyophilized NA gel isolate (ii), *Pseudomonas aeruginosa* biofilm (iii) and alkalinized and lyophilized *P. aeruginosa* biofilm (iv) showing the presence of diesterified phosphate peaks and the absence of monoesterified phosphate peaks for both NA gel isolate and biofilm in double distilled water, and the coexistence of diesterified and monoesterified phosphate peaks for both samples after alkalinization. This indicates that alkalinization of the matrix results in RNA transesterification. Micrographs of *P. aeruginosa* NA gel isolate stained green with (B) SYTO RNASelect showing RNA fibers and (C) TOTO-1 showing DNA fibers (scale bar 10 µm).

To visualize the DNA-RNA network organization, we used nucleic acid-specific stains, i.e. RNA specific SYTO RNASelect dye (Figure 4B) and the eDNA-specific TOTO-1 dye (Figure 4C) (Okshevsky and Meyer, 2014). Fibrous structures, which are typical of networked polymer gels (Cornwell and Smith, 2015), were observed in the NA gel isolate stained with both nucleic acid dyes as well as in the biofilm stained with the eDNA specific dye (Figure 1C). This is consistent with our observation that the biofilm is readily degraded by DNase I (Figure 1A) (Chen et al., 2004). Furthermore, the NA gel isolate was stained positively with the RNA-specific dye even after DNase I digestion, providing further evidence that RNA contributes to networking

bioRxiv preprint doi: https://doi.org/10.1101/527267; this version posted January 22, 2019. The copyright holder for this preprint (which was not certified by peer review) is the author/funder, who has granted bioRxiv a license to display the preprint in perpetuity. It is made available under aCC-BY 4.0 International license.

(Supplementary Figure 13). However, digestion with RNases III, A and H, did not degrade the biofilm (Figure 1A; Supplementary Figure 14). This may suggest that the RNase binding was shielded by hairpins in the network, or the presence of non-canonical DNA-RNA interactions (Geerts-Dimitriadou et al., 2012; Nakamura et al., 1991).

Non-canonical and Watson-Crick base pairs and tetrads support extracellular network.

Sequence analysis of the extracted material indicated that the gene coverage was even for both chromosomal and extracellular DNA with the exception of bacteriophage Pf1 genes (Supplementary Figure 15). However, the Pf1 knockout mutant of *P. aeruginosa* also displayed an elastic response when dissolved in EMIM-Ac (Supplementary Figure 16, Supplementary Tables 1 and 2), indicating that Pf1 DNA is unlikely to be responsible for the phase-separating behavior of *P. aeruginosa* biofilms. DNA and RNA interaction therefore cannot be explained by uneven gene coverage. To elucidate the mechanism of DNA-RNA gelation, we generated a 2D, through-space, ^{15}N-^{1}H HETCOR spectrum of ^{15}N labeled DNA-RNA gel isolated from a *P. aeruginosa* biofilm matrix (Figure 5A). This spectrum was run with longer cross polarization contact times so that correlations between distant ^{1}H and ^{15}N could be observed. This confirmed the complete absence of proteins and supported our conclusion that proteins do not contribute to the DNA-RNA interaction. The HETCOR spectrum showed four signal clusters at δ_H 10-14 ppm, and δ_N 140-160 ppm (Figure 5A), which arose from direct N-H couplings of T/U and G nucleobase imino groups. Two of these clusters (δ_H 12-14 ppm) resulted from imino protons hydrogen-bonded to a nucleobase nitrogen (i.e. N-H···N), and the other two (δ_H 10 -12 ppm) from imino protons hydrogen-bonded to a nucleobase carbonyl oxygen (i.e. N-H···O). Due to the longer cross polarization times we were able to observe a strong, long-range and indirect (i.e. intermolecular) correlation at δ_N 196 ppm arising from G-C Watson-Crick base pairing, i.e.

bioRxiv preprint doi: https://doi.org/10.1101/527267; this version posted January 22, 2019. The copyright holder for this preprint (which was not certified by peer review) is the author/funder, who has granted bioRxiv a license to display the preprint in perpetuity. It is made available under aCC-BY 4.0 International license.

C(N3)-G(H1). There was also a weak and indirect correlation at δ_N 220 ppm resulting from A-T/U Watson-Crick base pairing, i.e. A(N1) to U/T(H1).

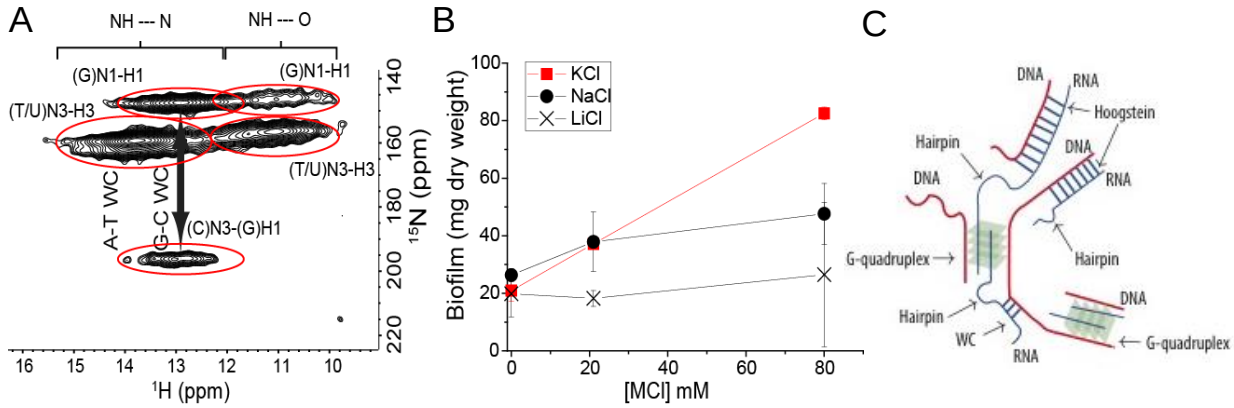

Figure 5: (A) Solid-state 2D ^{1}H-^{15}N through-space heteronuclear correlation (HETCOR) spectrum of extracellular nucleic acid (NA) gel isolate in double distilled water (2 mg), T = 25°C showing direct N-H couplings for G imino N (N3) and T/U imino N (N3) bonded to nucleobase nitrogen (NH···N). This indicates Watson-Crick (WC) G-C and U/T-A base pairings respectively; and for G imino N (N1) and T/U imino N (N3) bonded to nucleobase carbonyl oxygen (i.e. NH···O) indicating non-canonical G-G, G-T/U and U/T-U/T base pairings or tetrads. The spectrum also displayed indirect N-H correlations for the WC base pairs (i.e. C(N3) to G(H1) and A(N1) to U/T(H1)) and no indirect correlations for the non-canonical bonded nucleobases. The threshold for the A(N1)-T/U(H3) correlation was increased due to lower signal intensity for that particular coupling. (B) *Pseudomonas aeruginosa* biofilm growth yield at 37°C (5 d) as a function of [K^+], [Na^+] or [Li^+] showing the growth dependence on monovalent cation concentration (K^+>Na^+>Li^+). Error bars indicate standard deviation. (C) Illustration of how structural variability of RNA may allow for the formation of extracellular RNA and DNA networks through hairpins and a mixture of canonical and non-canonical base pairs or tetrads (i.e. Hoogsteen and G-quadruplexes).

The absence of long-range correlations between the clusters at δ_H 10 -12 ppm is consistent with non-Watson-Crick pairings for the G and T/U nucleobases. The observation of NH to O interactions suggests the formation of G-G, T/U-T/U, G-T/U Hoogsteen base pairs or tetrads.

bioRxiv preprint doi: https://doi.org/10.1101/527267; this version posted January 22, 2019. The copyright holder for this preprint (which was not certified by peer review) is the author/funder, who has granted bioRxiv a license to display the preprint in perpetuity. It is made available under aCC-BY 4.0 International license.

Hoogsteen H-bonded G-bases can assemble planarly into tetrads and self-stack to form G-quadruplexes (Hänsel-Hertsch et al., 2017). G-quadruplexes are stabilized by the presence of a monovalent cation, with potassium providing the greatest stability. We experimentally confirmed that potassium had a similar effect in a static biofilm growth assay. We found that potassium promoted *P. aeruginosa* biofilm growth to a greater extent than either sodium or lithium (Figure 5B). Additionally, this was a biofilm-specific effect as there was no effect of monovalent cation on planktonic growth (Supplementary Figure 17). Based on the SSNMR data coupled with the potassium effect and the earlier observation of several maxima in the CD spectrum of the NA gel isolate across the characteristic NA region of 250-285 nm, which suggested the coincidence of several NA conformations contributing to phase separation, it is proposed that G-quadruplexes contribute to extracellular DNA-RNA networking.

Discussion

We extracted a gel-forming complex composed of DNA and RNA from the extracellular matrix of *P. aeruginosa* biofilms without disrupting its fundamental structural or chemical organization. We report the novel observation that extracellular RNA contributes structurally to biofilms. While gel-forming exopolymers have been detected in other biofilms (Seviour et al., 2009), no functional DNA gel has been described for any biological system, much less one also including extracellular RNA.

While it is not possible to identify the precise nature of the DNA-RNA interaction based on the information presented here, purine-rich RNA as described here for the extracellular NA gel isolate (57 mol% A-G) is a characteristic of DNA-RNA duplexes because RNA purines bind more strongly to their DNA pyrimidine complement than vice versa (Nadel et al., 2015). Both Watson-Crick and non-canonical interactions were present in the NA gel isolate, which is also

bioRxiv preprint doi: https://doi.org/10.1101/527267; this version posted January 22, 2019. The copyright holder for this preprint (which was not certified by peer review) is the author/funder, who has granted bioRxiv a license to display the preprint in perpetuity. It is made available under aCC-BY 4.0 International license.

368 consistent with the discrepancy observed between RNA and DNA G+C mol% contents (Table
369 1). It is possible, therefore, that interactions between DNA and RNA, as described in this study,
370 account for the formation of a highly stable nucleic acid gel.

371 Non-canonical base pairing and hairpinning are commonly seen with RNA and cause multivalent
372 intermolecular interactions between RNA strands that lead to a sol-gel transition (Jain and Vale,
373 2017). The greater structural versatility of RNA could be a key to the ability of the eDNA to
374 form networks, with hairpins, as well as canonical and non-canonical base pair interactions all
375 contributing to the assembly of higher order NA structures (Figure 5C). RNA has recently been
376 found to promote intracellular phase separations, although this has not been extended to the
377 extracellular domain of prokaryotic cells (Shin and Brangwynne, 2017). Additionally, G-rich
378 RNA sequences are more predisposed to forming G-quadruplexes because they do not have a
379 complementary strand and in fact form more stable G-quadruplexes than DNA (Guo and Bartel,
380 2016). It is therefore probable that the RNA but not DNA enables DNA-RNA networking and
381 gelation.

382 The results presented here provide unprecedented resolution of the biofilm exopolymeric matrix
383 and its key foundation structural components. We have developed a methodology that preserved
384 the molecular organization of the foundational polymer in its native state upon extraction and
385 isolation. This enabled us to use SSNMR to describe intermolecular associations at the atomic
386 level.

387 Our findings that a DNA-RNA gel network can provide the foundation for biofilm matrices in *P.*
388 *aeruginosa* mark a departure from the prevailing paradigm that biofilm gelation is only due to
389 polysaccharides. The elastic and film-forming properties were also observed for *Pseudomonas*
390 *putida* and *Pseudomonas protegens* (Figs. S16 and S18; Supplementary Tables 1 and 2)

bioRxiv preprint doi: https://doi.org/10.1101/527267; this version posted January 22, 2019. The copyright holder for this preprint (which was not certified by peer review) is the author/funder, who has granted bioRxiv a license to display the preprint in perpetuity. It is made available under aCC-BY 4.0 International license.

391 suggesting that eDNA is broadly important for biofilm formation in members of this genus. In
392 addition to *Pseudomonas* spp., other organisms are known to have eDNA, including clinical
393 organisms *Staphylococcus aureus* (Mann et al., 2009), *Staphylococcus epidermidis* (Adam et al.,
394 2002), and *Mycobacterium abscessus* (Rose et al., 2015) as well as environmental isolates such
395 as strain F8 from the South Saskatchewan River (Böckelmann et al., 2006).

396 While eDNA is commonly thought to be the product of cell lysis, and has been shown to be
397 released by a sub-population of lytic *P. aeruginosa* cells (Turnbull et al., 2016), there is an
398 increasing awareness that it serves an important structural function, such as in activated sludge
399 granules (Cheng et al., 2011). Additionally, Bockelmann et al. (2006) observed that stable
400 filamentous networks produced by the aquatic strain F8 were comprised of DNA. This is the first
401 study that provides an explanation for how eDNA is organized structurally. However, the
402 environmental factors contributing to eDNA release and how this is regulated (i.e. whether it is
403 an active or passive process) are still unclear. It is possible that DNA-RNA foundational gel
404 networks, as described here for the Pseudomonads, are broad-scoping phenomena in biofilms,
405 and that interactions with RNA enable an extracellular structural function for DNA. Thus,
406 elucidating how nucleic acids, including RNA, are integral to the biophysical and other emergent
407 properties imparted on the biofilm via the extracellular matrix, will inform the regulation and
408 control of extracellular nucleic acid release across environmental and clinical biofilms.

409 ## Materials and Methods

410 ### Bacterial strains

411 Unless otherwise stated, all experiments were undertaken directly on *P. aeruginosa* PAO1
412 biofilms grown in lysogeny broth at 37°C. The *P. aeruginosa* PAO1 Δ*pf4* knockout mutant is a

bioRxiv preprint doi: https://doi.org/10.1101/527267; this version posted January 22, 2019. The copyright holder for this preprint (which was not certified by peer review) is the author/funder, who has granted bioRxiv a license to display the preprint in perpetuity. It is made available under aCC-BY 4.0 International license.

413 defined Pf4 chromosomal deletion mutant of the entire Pf4 prophage genome(Rice et al.,
414 2009).
415 *P. aeruginosa* PDO300, PDO300(*Δpel*) and PDO300(*Δpsl*) mutant strains were gratefully
416 received from Professor Bernd H. A. Rehm, Institute of Molecular Biosciences, Massey
417 University, New Zealand (Ghafoor et al., 2011). PDO300, PDO300(*Δpel*), PDO300(*Δpsl*) and
418 PAO1 (*Δpf4),* were also grown in LB at 37°C. *P. protogens Pf-5* and *P. putida* ATCC BAA-477
419 and S12 strain were were grown in LB at 30°C.

420 **Biofilm growth assay**

421 Ten milliliter aliquots of *P. aeruginosa* planktonic pre-cultures (LB, 200 rpm, 37°C, OD_{600} 2.40,
422 16 h) were diluted 50 times with LB in 2 L Erlenmeyer flasks and incubated for 5 d under static
423 conditions. Supplementary Figure 15A displays an image of 5-d old biofilm in LB. The cultures
424 were centrifuged at 10,000 x *g* for 15 min, the supernatant removed by decanting, and the
425 biofilm then collected and lyophilized (LabConco). Supplementary Figure 15B displays an
426 image of the culture after centrifugation showing clear separation of biofilm and supernatant.

427 **Enzymatic digestions**

428 Twenty milligrams of lyophilized biofilm was resuspended in 1 mL of either i) RNase buffer (50
429 mM Tris HCl, 10 mM EDTA, pH8) with 0.2 mg RNaseA from bovine pancreas (Sigma Aldrich),
430 ii) storage buffer (10 mM NaCl, 10 mM Tris-HCl) with 0.1 mg Pronase E from *Streptomyces*
431 *grisens* (Sigma Aldrich) with 0.5% (v/v), iii) 1X RNase H reaction buffer (20 mM Tris-HCl pH
432 7.8, 40 mM KCl, 8 mM MgCl2, 1 mM DTT) with 0.4 mg RNase H (Thermo Fisher Scientific),
433 iv) 1X RNase III reaction buffer (500 mM NaCl, 100 mM Tris pH 7.9, 100 mM MgCl2, 10 mM
434 DTT) with 0.6 mg RNase II (Thermo Fisher Scientific) or v) DNase I buffer (100mM Tris (pH
435 7.5), 25 mM $MgCl_2$ and $CaCl_2$) with 0.2 mg DNAse I from bovine pancreas (Sigma Aldrich). All

bioRxiv preprint doi: https://doi.org/10.1101/527267; this version posted January 22, 2019. The copyright holder for this preprint (which was not certified by peer review) is the author/funder, who has granted bioRxiv a license to display the preprint in perpetuity. It is made available under aCC-BY 4.0 International license.

digestions were performed with shaking at 200 rpm at 37°C for 16 h. The suspensions were then centrifuged (10,000 x *g*, 15 min), the supernatant was discarded and the pellets of the biofilm materials were lyophilized.

Normal force measurement

Forty milligrams per milliliter solutions of lyophilized biofilms were added to 1 mL 1-ethyl-3-methylimidazolium acetate and incubated in 55°C for either 2 h. A Haake Mars 3 (Thermo Fisher Scientific) stress-controlled rotational rheometer with Peltier controlled element at 25°C, was used for rheological measurements. Thirty five-illimeter diameter parallel plate geometry was used with smooth titanium plates to measure viscosity and normal stress difference ($N_1 - N_2$). Prior to measurement the gap error was zeroed at 4 N and gap error calculated as previously described (Bird et al., 1987; Davies and Stokes, 2008; Kravchuk and Stokes, 2013). One hundred microliters of sample was deposited on the plates. The plates were closed to 100 µm, the sample trimmed and the sample allowed to sit for 5 min prior to measurement. All measurements with Normal force (F_N) less than the resolution of the rheometer (i.e. < 0.1 N) were set to 0 before calculation of N_1-N_2 using equations 9-11, and viscosity from equation 3-5 in Davies and Stokes(Davies and Stokes, 2008) for the parallel plate geometry.

Only the linearly increasing portion of the normal stress difference curves are presented. Above this range normal stress difference begins to decrease again which may be due to elastic instabilities or associating polymers (Annable et al., 1993). Corrections were made to N_1 and $N_1 - N_2$ to account for inertia using equation 17 in Davies and Stokes (Davies and Stokes, 2008) and to correct for the baseline residual force in the samples. Except for the DNase I-treated biofilm, the shear rheology for all treatments could be modelled using the finitely extensible non-linear elastic with Gaussian closure proposed by Peterlin (FENE-P) constitutive model by varying four

bioRxiv preprint doi: https://doi.org/10.1101/527267; this version posted January 22, 2019. The copyright holder for this preprint (which was not certified by peer review) is the author/funder, who has granted bioRxiv a license to display the preprint in perpetuity. It is made available under aCC-BY 4.0 International license.

parameters to fit shear viscosity and normal stress difference as a function of shear rate (Supplementary Table 2). Fitting parameters for the FENE-P model include λ_1 = relaxation time, b = a measure of the relative extensibility of the model spring, η_s = solvent viscosity, η_p = polymer contribution to the viscosity. The FENE-P equations can be written in the following format, as shown by Bird et al.(1987):

$$\eta = \eta_s + \frac{\eta_p}{\lambda_1 \dot{\gamma}}\left((C_2 + C_1)^{\frac{1}{3}} - (C_2 - C_1)^{\frac{1}{3}}\right) \quad \text{(Equation 1)}$$

$$N_1 = \frac{2\eta_p}{\lambda_1}\left((C_2 + C_1)^{\frac{1}{3}} - (C_2 - C_1)^{\frac{1}{3}}\right)^2 \quad \text{(Equation 2)}$$

Where:

$$C_1 = \frac{b}{4}\lambda_1 \dot{\gamma} \quad \text{(Equation 3)}$$

$$C_2 = \left(C_1^2 + \left(\frac{b+3}{6}\right)^3\right)^{1/2} \quad \text{(Equation 4)}$$

All measurements were performed in triplicate. For clarity, one representative data set is presented in Figure 1A-B and Supplementary Figure 1A-B, with the respective Power Law and FENE-P model fit to that data set. Averaged values for the FENE-P and Power law fits, with the standard deviation across three replicates are shown in Supplementary Tables 1 and 2. Oscillatory measurements were carried out with controlled frequency 0.1 rad/s across an amplitude range of 0.01 to 10 %.

Extracellular polymeric substances (EPS) extraction

Lyophilized biofilms were dissolved in ionic liquid mixture (40% (v/v) 1-ethyl-3-methylimidazolium acetate (EMIM Ac): 60% (v/v) N,N-dimethyl acetamide (DMAc)) at 55°C

bioRxiv preprint doi: https://doi.org/10.1101/527267; this version posted January 22, 2019. The copyright holder for this preprint (which was not certified by peer review) is the author/funder, who has granted bioRxiv a license to display the preprint in perpetuity. It is made available under aCC-BY 4.0 International license.

for 16 h. The solution was centrifuged (10,000 x *g*) to remove any undissolved material. Perchloric acid (70%) was added (0.05% v/v) to the viscosified centrate (on ice). After 15 min incubation, the solution was centrifuged at 10,000 x *g* at 4°C for 15 min and the pellet recovered. This was repeated on the centrate two to four times until the solution was not viscous. The precipitate was dialysed against double distilled water for 2 d at 4°C (SnakeSkin™ Dialysis Tubing, 3.5K MWCO, 22 mm) and the retentate lyophilized (FreeZone Plus 4.5 Liter Cascade Benchtop Freeze Dry System). The same procedure was performed on calf thymus DNA, lipase, cytochrome C for the purposes of determining recovery yield of representative exoproteins, and on RNA from torula yeast for assessing by ^{31}P NMR whether the extraction procedure contributed to RNA transesterification (all from Sigma Aldrich).

Extracellular nucleic acid isolation

Twenty milligrams of lyophilized retentate (i.e. post perchloric acid precipitation) were dissolved in 1 mL of 40% (v/v) EMIM-Ac, 60% DMAc (v/v) (55°C, 16 h). Chromatographic separation was achieved in a Shimadzu system comprising DGU-20A 3r Prominence Degasser and LC-20AD Solvent Delivery Unit, fitted with two Agilent PLgel 10 µm column of 10^5Å pore size for separation across the MW range 200 kDa to 2000 kDa. The eluent flow rate was 3.0 mL.min^{-1} and the injection volume 1 mL. The fractions with molecular weight range of 2000-800kDa and 800-200kDa were pooled and dialyzed for 2 d at 4°C (SnakeSkin™ Dialysis Tubing, 3.5K MWCO, 22 mm) against double distilled water to induce gelation. The gel was then collected from the dialysis tubing.

Solution-state nuclear magnetic resonance (NMR)

Solution-state NMR experiments were performed on an 800 MHz Bruker Avance III spectrometer at 25^{o}C. Sample concentration was 10 mg (dry weight).mL^{-1} unless otherwise

bioRxiv preprint doi: https://doi.org/10.1101/527267; this version posted January 22, 2019. The copyright holder for this preprint (which was not certified by peer review) is the author/funder, who has granted bioRxiv a license to display the preprint in perpetuity. It is made available under aCC-BY 4.0 International license.

specified. Spectra were recorded either under conditions of neutral pH in 100% D_2O (Cambridge Isotope Laboratories), or following alkalinization (i.e. transesterification, 0.1 M NaOD, 55^{o}C, 2 h). 1-D NMR experiments include ^{1}H and ^{31}P direct detection, while 2-D NMR analysis include ^{13}C-HSQC, ^{13}C-HSQC-TOCSY, ^{1}H-^{31}P HETCOR, HMBC, and COSY. All spectral analyses were performed using Topspin and SPARKY software.

Asolectin (Sigma Aldrich) standard (10 mg/mL) and lyophilized *Pseudomonas aeruginosa* PAO1 biofilm (10mg/mL) were dissolved in 40% (v/v) EMIM Ac: 60% (v/v) DMAc at (55^{o}C, 2 h). *P. aeruginosa* PAO1 pre-culture cell lysate was prepared by lysing pre-culture cells with lysozyme in PBS. 10% (v/v) of D_2O was added to all samples for locking purposes.

Solid-state NMR

For solid-state NMR experiments performed on the NA gel isolate, ^{15}N labeled NH_4Cl-supplemented M9 minimal media was used for biofilm growth. M9 consisted of 9.552 g.L^{-1} $Na_2HPO_4.2H_2O$, 4.41g litre^{-1} KH_2PO_4, 1.71 g.L^{-1} NaCl, 1 g.L^{-1} $^{15}NH_4Cl$, 0.24 g.L^{-1} $MgSO_4$, 0.011 g.L^{-1} $CaCl_2$, 2 g.L^{-1} casamino acids, and 0.4 g.L^{-1} glucose. The NA gel was prepared from the M9-grown *P. aeruginosa* PAO1 biofilm as described above.

Solid-state NMR experiments were performed on 14.1 T Bruker Advance III instruments equipped with a 1.9 mm MAS probe operated in double mode. The typical ^{1}H, ^{15}N and ^{31}P $\pi/2$ pulse lengths were 2.3, 3.7, and 4.5 µs, respectively. 2D dipolar-based ^{15}N-^{1}H heteronulcear-correlation (HETCOR) experiments were conducted on the ^{15}N-labelled NA gel isolate at 37 kHz MAS spinning frequency. Variable temperature was regulated at -20ºC and the sample temperature was 12ºC (calibrated using ethylene glycol). In the ^{15}N-^{1}H HETCOR experiments, the initially excited ^{1}H magnetization was transferred to ^{15}N through a cross polarization step followed by t1 evolution. Then, the ^{15}N magnetization was flipped to longitudinal axis and 400

bioRxiv preprint doi: https://doi.org/10.1101/527267; this version posted January 22, 2019. The copyright holder for this preprint (which was not certified by peer review) is the author/funder, who has granted bioRxiv a license to display the preprint in perpetuity. It is made available under aCC-BY 4.0 International license.

ms proton saturation pulses were applied for water suppression. Subsequently, the ^{15}N magnetization was flipped to the transverse plane and transferred to ^{1}H via a second CP step for signal acquisition. Two ^{15}N-^{1}H HETCOR experiments were collected, one with 400 μs and the other with 2 ms contact times applied for both of the CP steps. Low power XiX ^{1}H decoupling (~10 kHz) was employed during ^{15}N evolution and WALTZ-16 decoupling (10 kHz) was implemented on ^{15}N channel during ^{1}H acquisition.

1-D ^{31}P experiments were performed on ^{15}N-labelled NA gel isolate and ^{15}N-labelled *P. aeruginosa* PAO biofilm, both directly after dialysis against double distilled water at 4°C for 2 d (SnakeSkin™ Dialysis Tubing, 3.5K MWCO, 22 mm), and following alkalinization (0.1 M NaOD, 55ºC, 15 min) and lyophilization (FreeZone Plus 4.5 Liter Cascade Benchtop Freeze Dry System). 15 kHz MAS spinning frequency and a sample temperature of 27ºC. 75 kHz SPINAL64 ^{1}H decoupling was applied during ^{31}P acquisition time. All chemical shifts were indirectly referenced using adamantane as a secondary standard (downfield peak is at 40.48 ppm, DSS scale).

Monovalent cation-dependent biofilm growth

Ten milliliters aliquots of *P. aeruginosa* pre-cultures (supplemented M9, 200 rpm, OD_{600} 2.40, 16 h) were transferred into 500 mL M9 minimal media (8.5 $g.L^{-1}$ $Na_2HPO_4.2H_2O$, 2.0 $g.L^{-1}$ of $NaH_2PO_4.H_2O$, 1.0 $g.L^{-1}$ KH_2PO_4, 1.0 $g.L^{-1}$ NH_4Cl, 0.48 $g.L^{-1}$ $MgSO_4$, 0.011 $g.L^{-1}$ $CaCl_2$, 2 $g.L^{-1}$ casamino acids, and 0.4 $g.L^{-1}$ glucose) supplemented with either KCl, LiCl or NaCl at either of three different concentrations (0, 0.02 mM and 0.08 mM). Biofilms were collected by centrifugation (10,000 x g, 15 min) as described above, lyophilized (LabConco) and weighed. To describe the growth curve, *P. aeruginosa* wild type PAO1 pre-culture was incubated in M9 media at 37°C, 200 rpm for 16 h. PAO1 WT pre-culture was then diluted with supplemented M9

bioRxiv preprint doi: https://doi.org/10.1101/527267; this version posted January 22, 2019. The copyright holder for this preprint (which was not certified by peer review) is the author/funder, who has granted bioRxiv a license to display the preprint in perpetuity. It is made available under aCC-BY 4.0 International license.

media to a volume of 75 mL and a starting OD_{600} of 0.01, in a 250 mL Erlenmeyer flask. The mixture was incubated at 37°C with shaking (200rpm). The OD_{600} of the bacteria was measured hourly for 9 h followed by final time point at 24 h.

DNA Sequencing

Genomic DNA was extracted from the biofilm using FastDNA SPIN Kit for soil (MP Biomedicals, USA) as per the standard protocol. Briefly, biofilm was resuspended in Sodium Phosphate Buffer in was lysed (Lysing Matrix), homogenized (FastPrep®, 40 seconds, speed setting 6.0), and the cell debris removed by centrifugation (14,000 x *g*, 5 min). Proteins were removed by precipitation (250 µl Protein Precipitation Solution), the supernatant mixed with DNA Binding Matrix, which was then homogenized and transferred to a SPIN™ Filter. Excess supernatant was removed by centrifugation (14,000 x *g*, 5 min). DNA was then eluted from air dried DNA Binding Matrix with DNase/ Pyrogen-Free Water.

The NA gel isolate was resuspended in 500 uL of 1x Protease K solution (10× Protease K solution: 10 mM Tris HCl, 1% SDS and 10 mM EDTA, pH 8 buffer (10× protease K buffer containing 500 mM Tris-HCl, 10% SDS, 10 mM $CaCl_2$) and 10 µL of Protease K (20 $mg.mL^{-1}$, Thermo Fisher Scientific) was added and the mixture incubated at 56°C for 2-16 h, after which DNA was extracted as previously described in the phenol-chloroform method(Ausubel, 2002). Samples before sequencing were further purified to remove any remaining protein and RNA by RNase and Proteinase K treatment. The DNA was then isolated using phenol-chloroform precipitation as described above. The DNA precipitate was dissolved in TE buffer, the purity confirmed by 260/280 value in Nanodrop (acceptable range value: 1.8-2.0) and Qubit® 2.0 fluorometer.

bioRxiv preprint doi: https://doi.org/10.1101/527267; this version posted January 22, 2019. The copyright holder for this preprint (which was not certified by peer review) is the author/funder, who has granted bioRxiv a license to display the preprint in perpetuity. It is made available under aCC-BY 4.0 International license.

571 The molecular weight distributions of extracellular and genomic DNA were measured on a 1%
572 agarose gel, which was prepared from Viviantis LE grade agarose using 1x TAE buffer (40 mM
573 Tris, 20 mM Acetate and 1 mM EDTA, pH 8.6). Gels were run horizontally. After
574 electrophoresis, the gel was stained for 0.5 h with ethidium bromide and visualized under
575 UV(Lee et al., 2012).
576 Three replicates were used for each DNA sequence analysis. Library was produced using
577 Illumina DNA sample preparation kit. The libraries were sequenced using Illumina MiSeq
578 platform (Illumina, San Diego, Ca) with paired-end protocol to read lengths of 600 nt generating
579 a total of 1,614,106 and 1,848,846 paired end reads. Raw reads were quality filtered (reads
580 remaining after trimming: PPG1-1549104, PBLC1-1666280) and aligned to the *P. aeruginosa*
581 PAO1 (AE004091) genome using CLC Genomics Workbench 9.0 (CLC bio, Cambridge, MA).

582 **Circular Dichroism CD**

583 Five-day old biofilm and NA gel isolate were resuspended in double distilled water to achieve
584 UV absorbance reading 1 and ddH_2O served as a blank. The heat-treated samples were analyzed
585 by JASCO-815 spectropolarimeter in a 1 cm path length quartz cuvette containing a solution
586 volume 500 µL. Spectra (200-320 nm) were measured at 1°C increments from 30 - 90°C. For
587 each measurement, an average of three scans was taken and the buffer spectra subtracted. Each
588 spectrum presented is the rolling average across 5 temperatures.

589 **Staining and microscopy**

590 Microscopic imaging was conducted on a confocal microscope Zeiss LSM 780 with a 63×
591 objective. Extracellular RNA in the gel isolate were stained using SYTO RNASelect (Thermo
592 Fisher Scientific) green fluorescent cell stain (5 mM solution in DMSO). Five µM stain solution
593 was prepared from 1 µL of stock in 1X PBS solution (137 mM NaCl**,** 2.7 mM KCl**,** 4.3 mM

bioRxiv preprint doi: https://doi.org/10.1101/527267; this version posted January 22, 2019. The copyright holder for this preprint (which was not certified by peer review) is the author/funder, who has granted bioRxiv a license to display the preprint in perpetuity. It is made available under aCC-BY 4.0 International license.

Na_2HPO_4, 1.47 mM KH_2PO_4). The gel isolate was labelled with 5 µM stain solution, kept at 37°C for 20 min and then transferred to glass side for imaging.

eDNA staining was achieved by depositing biofilm or NA gel isolate on a glass slide, air-drying overnight and incubating with 2 µM TOTO-1 iodide (1 mM solution in DMSO, Thermo Fisher Scientific) for 15 min.

Acknowledgments

We acknowledge Prof Bernd Rehm for supplying polysaccharide deletion mutants of *P. aeruginosa*, Dan Roizman for providing *P. putida*, Long Yu for assistance with rheology, Dr Gleb Yakubov for coordinating sample preparation for rheological measurements, Ravi Jagadeeshan for discussion regarding DNA normal force analysis, and Florentin Constancias for analyzing the sequencing data. SCELSE is funded by Singapore's Ministry of Education, National Research Federation, Nanyang Technological University (NTU), and National University of Singapore (NUS) and hosted by NTU in partnership with NUS.

Author Contributions

T.S., F.R.W., W.L.L., S.M., H.M.S. and X.S. performed experiments; T.S. and A.T.P. designed the experiments. T.S., F.R.W., A.T.P., H.M.S., G.S.K. and J.R.S. analysed the data. T.S., F.R.W., W.L.L., H.M.S., S.A.R., A.T.P and S.K. wrote the manuscript.

Competing Interests

All authors have no competing interests.

References

Mixed species biofilms of Candida albicans and Staphylococcus epidermidis
B Adam, GS Baillie, LJ Douglas (2002)

bioRxiv preprint doi: https://doi.org/10.1101/527267; this version posted January 22, 2019. The copyright holder for this preprint (which was not certified by peer review) is the author/funder, who has granted bioRxiv a license to display the preprint in perpetuity. It is made available under aCC-BY 4.0 International license.

Journal of Medical Microbiology **51**:344-349.
doi:10.1099/0022-1317-51-4-344

A characterization of DNA release in *Pseudomonas aeruginosa* cultures and biofilms
M Allesen-Holm, KB Barken, L Yang, M Klausen, JS Webb, S Kjelleberg, S Molin, M Givskov, T Tolker-Nielsen (2006)
Molecular Microbiology **59**:1114-1128.
doi:10.1111/j.1365-2958.2005.05008.x

The rheology of solutions of associating polymers: Comparison of experimental behavior with transient network theory
T Annable, R Buscall, R Ettelaie, D Whittlestone (1993)
Journal of Rheology **37**:695-726.
doi:10.1122/1.550391

Short protocols in molecular biology : a compendium of methods from Current protocols in molecular biology
FM Ausubel (2002)
5th ed. New York: Wiley.

Dynamics of Polymeric Liquids
RB Bird, RC Armstrong, O Hassager (1987)
2nd ed.

Bacterial extracellular DNA forming a defined network-like structure
U Böckelmann, A Janke, R Kuhn, TR Neu, J Wecke, JR Lawrence, U Szewzyk (2006)
FEMS Microbiology Letters **262**:31-38.
doi:10.1111/j.1574-6968.2006.00361.x

Infections caused by *Pseudomonas aeruginosa*
GP Bodey, R Bolivar, V Fainstein, L Jadeja (1983)
Review of Infectious Diseases **5**:279-313.
doi:10.1093/clinids/5.2.279

***Pseudomonas aeruginosa* uses a cyclic-di-GMP-regulated adhesin to reinforce the biofilm extracellular matrix**
BR Borlee, AD Goldman, K Murakami, R Samudrala, DJ Wozniak, MR Parsek (2010)
Molecular Microbiology **75**:827-842.
doi:10.1111/j.1365-2958.2009.06991.x

DNA/RNA helicase gene mutations in a form of juvenile amyotrophic lateral sclerosis (ALS4)
YZ Chen, CL Bennett, HM Huynh, IP Blair, I Puls, J Irobi, I Dierick, A Abel, ML Kennerson, BA Rabin, GA Nicholson, M Auer-Grumbach, K Wagner, P De Jonghe, JW Griffin, KH Fischbeck, V Timmerman, DR Cornblath, PF Chance (2004)
Am J Hum Genet **74**:1128-1135.
doi:10.1086/421054

Evidence of compositional differences between the extracellular and intracellular DNA of a granular sludge biofilm
M Cheng, AE Cook, T Fukushima, PL Bond (2011)
Letters in Applied Microbiology **53**:1-7.
doi:doi:10.1111/j.1472-765X.2011.03074.x

Dynamic Remodeling of Microbial Biofilms by Functionally Distinct Exopolysaccharides
SC Chew, B Kundukad, T Seviour, JRC Van Der Maarel, L Yang, SA Rice, P Doyle, S Kjelleberg (2014)
mBio **5**:e01536-01514.
doi:10.1128/mBio.01536-14

The Pel and Psl polysaccharides provide *Pseudomonas aeruginosa* structural redundancy within the biofilm matrix
KM Colvin, Y Irie, CS Tart, R Urbano, JC Whitney, C Ryder, PL Howell, DJ Wozniak, MR Parsek (2012)
Environmental Microbiology **14**:1913-1928.
doi:10.1111/j.1462-2920.2011.02657.x

Expanding the scope of gels - Combining polymers with low-molecular-weight gelators to yield modified self-assembling smart materials with high-tech applications
DJ Cornwell, DK Smith (2015)
Materials Horizons **2**:279-293.
doi:10.1039/c4mh00245h

bioRxiv preprint doi: https://doi.org/10.1101/527267; this version posted January 22, 2019. The copyright holder for this preprint (which was not certified by peer review) is the author/funder, who has granted bioRxiv a license to display the preprint in perpetuity. It is made available under aCC-BY 4.0 International license.

Thin film and high shear rheology of multiphase complex fluids
GA Davies, JR Stokes (2008)
Journal of Non-Newtonian Fluid Mechanics **148**:73-87.
doi:10.1016/j.jnnfm.2007.04.013
Kinetic model of a granular sludge SBR: Influences on nutrient removal
MK De Kreuk, C Picioreanu, M Hosseini, JB Xavier, MCM Van Loosdrecht (2007)
Biotechnology and Bioengineering **97**:801-815.
doi:10.1002/bit.21196
G-Quadruplex secondary structure obtained from circular dichroism spectroscopy
R Del Villar-Guerra, JO Trent, JB Chaires (2018)
Angewandte Chemie International Edition **57**:7171-7175.
doi:doi:10.1002/anie.201709184
Biofilm streamers cause catastrophic disruption of flow with consequences for environmental and medical systems
K Drescher, Y Shen, BL Bassler, HA Stone (2013)
Proceedings of the National Academy of Sciences of the United States of America **110**:4345-4350.
doi:10.1073/pnas.1300321110
The biofilm matrix
H-C Flemming, J Wingender (2010)
Nature Reviews Microbiology **8**:623-633.
doi:10.1038/nrmicro2415
Two genetic loci produce distinct carbohydrate-rich structural components of the *Pseudomonas aeruginosa* biofilm matrix
L Friedman, R Kolter (2004)
Journal of Bacteriology **186**:4457-4465.
doi:10.1128/jb.186.14.4457-4465.2004
Analysis of the Tomato spotted wilt virus Ambisense S RNA-Encoded Hairpin Structure in Translation
C Geerts-Dimitriadou, Y-Y Lu, C Geertsema, R Goldbach, R Kormelink (2012)
PLOS ONE **7**:e31013.
doi:10.1371/journal.pone.0031013
Role of exopolysaccharides in *Pseudomonas aeruginosa* biofilm formation and architecture
A Ghafoor, ID Hay, BHA Rehm (2011)
Applied and Environmental Microbiology **77**:5238-5246.
doi:10.1128/aem.00637-11
Using circular dichroism spectra to estimate protein secondary structure
NJ Greenfield (2006)
Nature protocols **1**:2876-2890.
doi:10.1038/nprot.2006.202
RNA G-quadruplexes are globally unfolded in eukaryotic cells and depleted in bacteria
JU Guo, DP Bartel (2016)
Science **353**:aaf5371.
doi:10.1126/science.aaf5371
DNA G-quadruplexes in the human genome: detection, functions and therapeutic potential
R Hänsel-Hertsch, M Di Antonio, S Balasubramanian (2017)
Nature Reviews Molecular Cell Biology **18**:279.
doi:10.1038/nrm.2017.3
Major proteomic changes associated with amyloid-induced biofilm formation in *Pseudomonas aeruginosa* PAO1
F-A Herbst, MT Søndergaard, H Kjeldal, A Stensballe, PH Nielsen, MS Dueholm (2015)
Journal of Proteome Research **14**:72-81.
doi:10.1021/pr500938x
Antibiotic resistance of bacterial biofilms
N Høiby, T Bjarnsholt, M Givskov, SR Molin, O Ciofu (2010)
International Journal of Antimicrobial Agents **35**:322-332.
doi:10.1016/j.ijantimicag.2009.12.011
Self-produced exopolysaccharide is a signal that stimulates biofilm formation in *Pseudomonas aeruginosa*

bioRxiv preprint doi: https://doi.org/10.1101/527267; this version posted January 22, 2019. The copyright holder for this preprint (which was not certified by peer review) is the author/funder, who has granted bioRxiv a license to display the preprint in perpetuity. It is made available under aCC-BY 4.0 International license.

Y Irie, BR Borlee, JR O'connor, PJ Hill, CS Harwood, DJ Wozniak, MR Parsek (2012)
Proceedings of the National Academy of Sciences of the United States of America **109**:20632-20636.
doi:10.1073/pnas.1217993109
RNA phase transitions in repeat expansion disorders
A Jain, RD Vale (2017)
Nature **546**:243-247.
doi:10.1038/nature22386
Pel is a cationic exopolysaccharide that cross-links extracellular DNA in the *Pseudomonas aeruginosa* biofilm matrix
LK Jennings, KM Storek, HE Ledvina, C Coulon, LS Marmont, I Sadovskaya, PR Secor, BS Tseng, M Scian, A Filloux, DJ Wozniak, PL Howell, MR Parsek (2015)
Proceedings of the National Academy of Sciences of the United States of America **112**:11353-11358.
doi:10.1073/pnas.1503058112
A phenomenological model for predicting melting temperatures of DNA sequences
G Khandelwal, J Bhyravabhotla (2010)
PLOS ONE **5**:e12433.
doi:10.1371/journal.pone.0012433
Review of algorithms for estimating the gap error correction in narrow gap parallel plate rheology
O Kravchuk, JR Stokes (2013)
Journal of Rheology **57**:365-375.
doi:10.1122/1.4774323
Analysis of the ion adsorption–desorption characteristics of biofilm matrices
A Kurniawan, T Yamamoto, Y Tsuchiya, H Morisaki (2012)
Microbes and Environments **27**:399-406.
doi:10.1264/jsme2.ME11339
Circular dichroism and conformational polymorphism of DNA
J Kypr, I Kejnovská, D Renčiuk, M Vorlíčková (2009)
Nucleic Acids Research **37**:1713-1725.
doi:10.1093/nar/gkp026
Agarose gel electrophoresis for the separation of DNA fragments
PY Lee, J Costumbrado, C-Y Hsu, YH Kim (2012)
Journal of Visualized Experiments : JoVE 3923.
doi:10.3791/3923
Modulation of eDNA release and degradation affects *Staphylococcus aureus* biofilm maturation
EE Mann, KC Rice, BR Boles, JL Endres, D Ranjit, L Chandramohan, LH Tsang, MS Smeltzer, AR Horswill, KW Bayles (2009)
PLoS One **4**:e5822.
doi:10.1371/journal.pone.0005822
Persistent draining crossover in DNA and other semi-flexible polymers: Evidence from hydrodynamic models and extensive measurements on DNA solutions
ML Mansfield, A Tsortos, JF Douglas (2015)
The Journal of Chemical Physics **143**:124903.
doi:10.1063/1.4930918
RNA structure determination by solid-state NMR spectroscopy
A Marchanka, B Simon, G Althoff-Ospelt, T Carlomagno (2015)
Nature Communications **6**:7024.
doi:10.1038/ncomms8024
RNA:DNA hybrids in the human genome have distinctive nucleotide characteristics, chromatin composition, and transcriptional relationships
J Nadel, R Athanasiadou, C Lemetre, NA Wijetunga, P Ó Broin, H Sato, Z Zhang, J Jeddeloh, C Montagna, A Golden, C Seoighe, JM Greally (2015)
Epigenetics & Chromatin **8**:46.
doi:10.1186/s13072-015-0040-6
How does RNase H recognize a DNA.RNA hybrid?
H Nakamura, Y Oda, S Iwai, H Inoue, E Ohtsuka, S Kanaya, S Kimura, C Katsuda, K Katayanagi, K Morikawa (1991)

bioRxiv preprint doi: https://doi.org/10.1101/527267; this version posted January 22, 2019. The copyright holder for this preprint (which was not certified by peer review) is the author/funder, who has granted bioRxiv a license to display the preprint in perpetuity. It is made available under aCC-BY 4.0 International license.

Proceedings of the National Academy of Sciences **88**:11535-11539.

Evaluation of fluorescent stains for visualizing extracellular DNA in biofilms
M Okshevsky, RL Meyer (2014)
Journal of Microbiological Methods **105**:102-104.
doi:10.1016/j.mimet.2014.07.010

The role of extracellular DNA in the establishment, maintenance and perpetuation of bacterial biofilms
M Okshevsky, RL Meyer (2015)
Critical Reviews in Microbiology **41**:341-352.
doi:10.3109/1040841x.2013.841639

Molecular mechanisms of biofilm infection: biofilm virulence factors
PL Phillips, GS Schultz (2012)
Advances in Wound Care **1**:109-114.
doi:10.1089/wound.2011.0301

Molecular simulations of RNA 2′ -o-transesterification reaction models in solution
BK Radak, ME Harris, DM York (2013)
The Journal of Physical Chemistry B **117**:94-103.
doi:10.1021/jp3084277

Solid-state NMR for bacterial biofilms
C Reichhardt, L Cegelski (2014)
Molecular physics **112**:887-894.
doi:10.1080/00268976.2013.837983

The biofilm life cycle and virulence of *Pseudomonas aeruginosa* are dependent on a filamentous prophage
SA Rice, CH Tan, PJ Mikkelsen, V Kung, J Woo, M Tay, A Hauser, D Mcdougald, JS Webb, S Kjelleberg (2009)
The ISME journal **3**:271-282.
doi:10.1038/ismej.2008.109

***Mycobacterium avium* possesses extracellular DNA that contributes to biofilm formation, structural integrity, and tolerance to antibiotics**
SJ Rose, LM Babrak, LE Bermudez (2015)
PLOS ONE **10**:e0128772.
doi:10.1371/journal.pone.0128772

Shear thickening in filled Boger fluids
R Scirocco, J Vermant, J Mewis (2005)
Journal of Rheology **49**:551-567.
doi:10.1122/1.1849185

Functional amyloids keep quorum-sensing molecules in check
T Seviour, SH Hansen, L Yang, YH Yau, VB Wang, MR Stenvang, G Christiansen, E Marsili, M Givskov, Y Chen, DE Otzen, PH Nielsen, S Geifman-Shochat, S Kjelleberg, MS Dueholm (2015a)
Journal of Biological Chemistry **290**:6457-6469.
doi:10.1074/jbc.M114.613810

Selectively inducing the synthesis of a key structural exopolysaccharide in aerobic granules by enriching for *Candidatus* 'Competibacter phosphatis'
T Seviour, LK Lambert, M Pijuan, Z Yuan (2011)
Applied Microbiology and Biotechnology **92**:1297-1305.
doi:10.1007/s00253-011-3385-1

Molecular dynamics unlocks atomic level self-assembly of the exopolysaccharide matrix of water-treatment granular biofilms
T Seviour, AK Malde, S Kjelleberg, Z Yuan, AE Mark (2012)
Biomacromolecules **13**:1965-1972.
doi:10.1021/bm3005808

Gel-forming exopolysaccharides explain basic differences between structures of aerobic sludge granules and floccular sludges
T Seviour, M Pijuan, T Nicholson, J Keller, Z Yuan (2009)
Water Research **43**:4469-4478.
doi:10.1016/j.watres.2009.07.018

Solvent optimization for bacterial extracellular matrices: a solution for the insoluble
T Seviour, P Weerachanchai, J Hinks, D Roizman, SA Rice, L Bai, J-M Lee, S Kjelleberg (2015b)

bioRxiv preprint doi: https://doi.org/10.1101/527267; this version posted January 22, 2019. The copyright holder for this preprint (which was not certified by peer review) is the author/funder, who has granted bioRxiv a license to display the preprint in perpetuity. It is made available under aCC-BY 4.0 International license.

RSC Advances **5**:7469-7478.
doi:10.1039/c4ra10930a

Extensive genomic plasticity in *Pseudomonas aeruginosa* revealed by identification and distribution studies of novel genes among clinical isolates
K Shen, S Sayeed, P Antalis, J Gladitz, A Ahmed, B Dice, B Janto, R Dopico, R Keefe, J Hayes, S Johnson, S Yu, N Ehrlich, J Jocz, L Kropp, R Wong, RM Wadowsky, M Slifkin, RA Preston, G Erdos, JC Post, GD Ehrlich, FZ Hu (2006)
Infection and Immunity **74**:5272-5283.
doi:10.1128/IAI.00546-06

Liquid phase condensation in cell physiology and disease
Y Shin, CP Brangwynne (2017)
Science **357**:doi:10.1126/science.aaf4382

Swirling flow of viscoelastic fluids. Part 2. Elastic effects
JR Stokes, LJW Graham, NJ Lawson, DV Boger (2001)
Journal of Fluid Mechanics **429**:117-153.
doi:10.1017/S0022112000002901

Explosive cell lysis as a mechanism for the biogenesis of bacterial membrane vesicles and biofilms
L Turnbull, M Toyofuku, AL Hynen, M Kurosawa, G Pessi, NK Petty, SR Osvath, G Carcamo-Oyarce, ES Gloag, R Shimoni, U Omasits, S Ito, X Yap, LG Monahan, R Cavaliere, CH Ahrens, IG Charles, N Nomura, L Eberl, CB Whitchurch (2016)
Nature Communications **7**:11220.
doi:10.1038/ncomms11220

Extended dissolution studies of cellulose in imidazolium based ionic liquids
J Vitz, T Erdmenger, C Haensch, US Schubert (2009)
Green Chemistry **11**:417-424.
doi:10.1039/b818061j

NMR of proteins and nucleic acids
K Wüthrich (2008)
2nd ed. New York: John Wiley and Sons.

DNA stability in ionic liquids and deep eutectic solvents
H Zhao (2015)
Journal of Chemical Technology & Biotechnology **90**:19-25.
doi:doi:10.1002/jctb.4511

bioRxiv preprint doi: https://doi.org/10.1101/527267; this version posted January 22, 2019. The copyright holder for this preprint (which was not certified by peer review) is the author/funder, who has granted bioRxiv a license to display the preprint in perpetuity. It is made available under aCC-BY 4.0 International license.

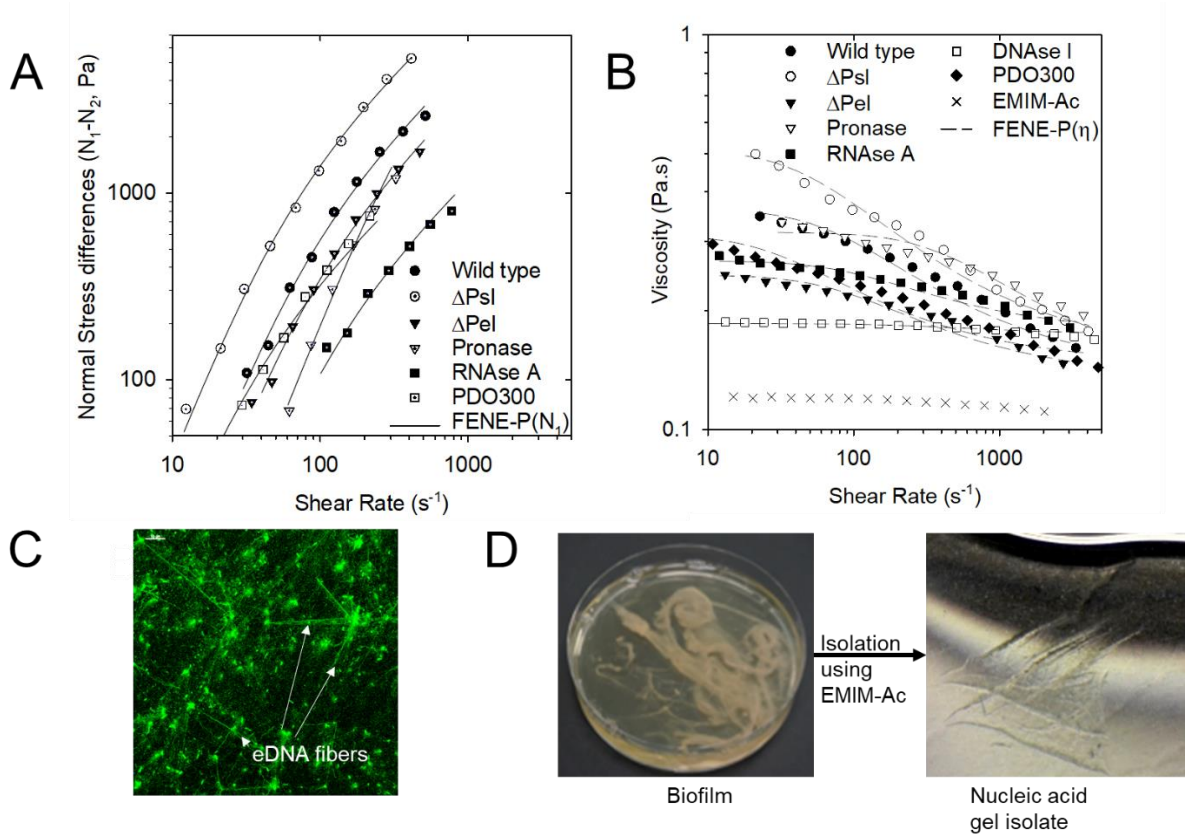

Figure 1: (A) N_1-N_2 and (B) viscosity against shear rate for *Pseudomonas aeruginosa* biofilm wild type, PDO300, ΔPsl, ΔPel, and pronase, RNase A and DNase I digested wild type biofilm immediately following dissolution in 1-ethyl-3-methylimidazolium acetate (40 mg/mL) at 25 °C, 100 µm gap. This is measured as a function of shear stress from 10 to 1000 Pa. (N_1 –N_2) is not described for DNase I digested biofilm in Figure 1A and Supplementary Figure 1B as their normal force (F_N) is less than the resolution of the rheometer (i.e. 0.1 N) and set to zero for calculating (N_1 –N_2). Both the N_1-N_2 and viscosity data are fitted with the FENE-P model, a rigid dumbell model for polymer solutions. Fitting parameters are shown in Supplementary Table 2. (C) Micrograph of *P. aeruginosa* biofilm DNA stained green with TOTO-1 (scale bar 10 µm). (D) Phase separation of extracellular nucleic acids extracted from *P. aeruginosa* biofilms into a gel occurs upon transfer from 1-ethyl-3-methylimidazolium acetate into water.

bioRxiv preprint doi: https://doi.org/10.1101/527267; this version posted January 22, 2019. The copyright holder for this preprint (which was not certified by peer review) is the author/funder, who has granted bioRxiv a license to display the preprint in perpetuity. It is made available under aCC-BY 4.0 International license.

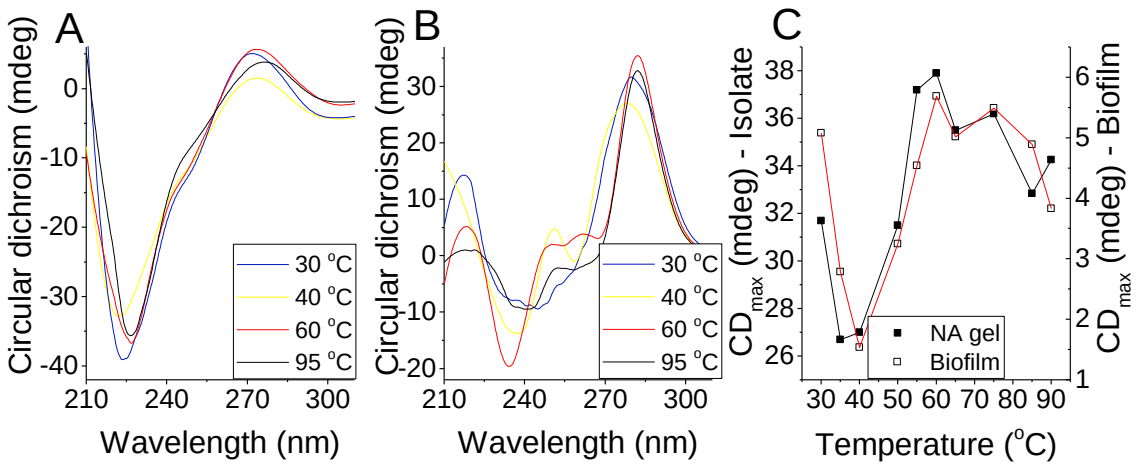

Figure 2: Circular dichroism (CD) spectra of (A) *Pseudomonas aeruginosa* biofilm and (B) extracellular nucleic acids (NA) gel isolate at temperatures between 30 and 95°C. (C) Amplitude of dominant NA peak, CD_{max} (260-285 nm), from CD spectra of *P. aeruginosa* biofilm (seen in (A)) and its extracted extracellular nucleic acid gel (seen in (B)) from T = 30°C to T = 95°C.

bioRxiv preprint doi: https://doi.org/10.1101/527267; this version posted January 22, 2019. The copyright holder for this preprint (which was not certified by peer review) is the author/funder, who has granted bioRxiv a license to display the preprint in perpetuity. It is made available under aCC-BY 4.0 International license.

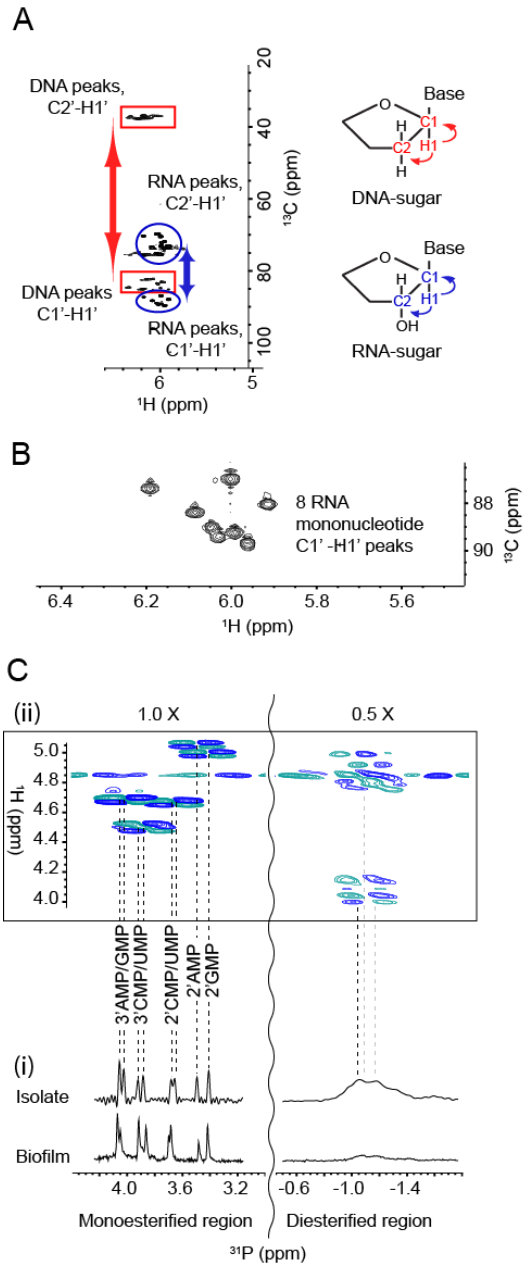

Figure 3: (A) Nuclear magnetic resonance (NMR) ^{1}H-^{13}C heteronuclear single quantum coherence (HSQC)-total correlation spectroscopy (TOCSY) spectrum at 25°C of extracellular nucleic acids (NA) gel isolate after alkalinization showing the C1'-H1' cross peaks of RNA (blue ovals) and DNA (red rectangles) and their correlations to the neighboring carbon C2'-H1'. Schematics (right) illustrate these correlations. (B) ^{1}H-^{13}C HSQC spectrum of extracellular NA gel isolate at 25°C after alkalinization identifying eight monoribonucleic acid ribose spin systems. (C) 1-D ^{31}P NMR of NA isolate gel and *Pseudomomonas aeruginosa* biofilm with proton decoupling showing the presence of monoesterified (i.e. monoribonucleotides) and diesterified (i.e. DNA) phosphate peaks (i), and 2-D ^{1}H-^{31}P heteronuclear correlation (HETCOR) spectrum of extracellular NA showing the ^{31}P-^{1}H cross-peaks of monoribonucleotides and DNA (ii). Couplings of monoesterified phosphates to H2' or H3' of eight monoesterified monoribonucleotides (from left to right: 3' AMP/3' GMP, 3' CMP/3' UMP, 2' CMP/2' UMP, 2' AMP, 2' GMP); and diesterified phosphate to DNA H3' and H5'/H5'' protons, are denoted by the dashed lines. There is a discontinuity (wavy line) in the ^{31}P axis due to the different thresholds required to illustrate the ^{31}P-^{1}H correlations in the mono-esterified and di-esterified regions. All samples were prepared in 0.1 M NaOD (10 mg/mL) and preheated to 55°C for 2 h.

bioRxiv preprint doi: https://doi.org/10.1101/527267; this version posted January 22, 2019. The copyright holder for this preprint (which was not certified by peer review) is the author/funder, who has granted bioRxiv a license to display the preprint in perpetuity. It is made available under aCC-BY 4.0 International license.

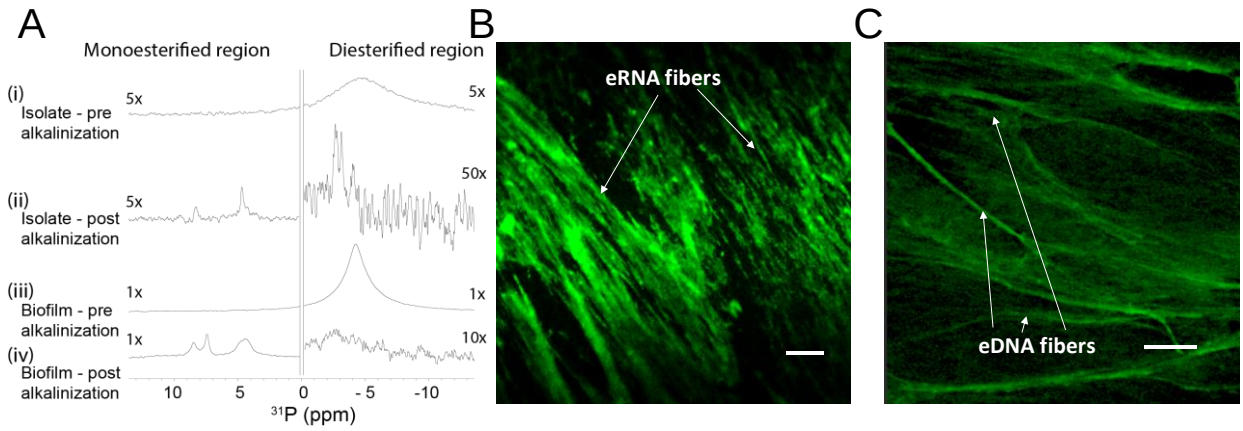

Figure 4: (A) Solid-state ^{31}P NMR spectra at T = 25°C of extracellular NA gel isolate (i), alkalinized and lyophilized NA gel isolate (ii), *Pseudomonas aeruginosa* biofilm (iii) and alkalinized and lyophilized *P. aeruginosa* biofilm (iv) showing the presence of diesterified phosphate peaks and the absence of monoesterified phosphate peaks for both NA gel isolate and biofilm in double distilled water, and the coexistence of diesterified and monoesterified phosphate peaks for both samples after alkalinization. This indicates that alkalinization of the matrix results in RNA transesterification. Micrographs of *P. aeruginosa* NA gel isolate stained green with (B) SYTO RNASelect showing RNA fibers and (C) TOTO-1 showing DNA fibers (scale bar 10 µm).

bioRxiv preprint doi: https://doi.org/10.1101/527267; this version posted January 22, 2019. The copyright holder for this preprint (which was not certified by peer review) is the author/funder, who has granted bioRxiv a license to display the preprint in perpetuity. It is made available under aCC-BY 4.0 International license.

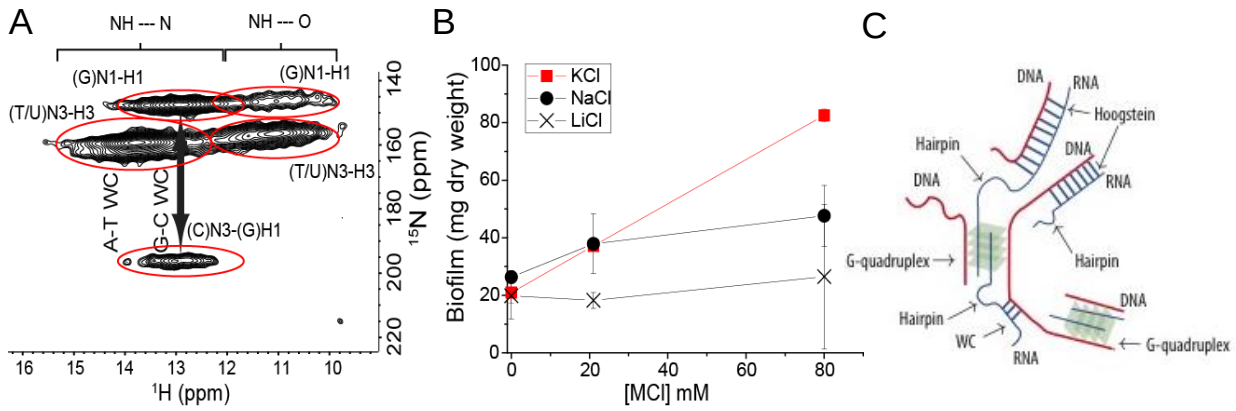

Figure 5: (A) Solid-state 2D ^{1}H-^{15}N through-space heteronuclear correlation (HETCOR) spectrum of extracellular nucleic acid (NA) gel isolate in double distilled water (2 mg), T = 25°C showing direct N-H couplings for G imino N (N3) and T/U imino N (N3) bonded to nucleobase nitrogen (NH···N). This indicates Watson-Crick (WC) G-C and U/T-A base pairings respectively; and for G imino N (N1) and T/U imino N (N3) bonded to nucleobase carbonyl oxygen (i.e. NH···O) indicating non-canonical G-G, G-T/U and U/T-U/T base pairings or tetrads. The spectrum also displayed indirect N-H correlations for the WC base pairs (i.e. C(N3) to G(H1) and A(N1) to U/T(H1)) and no indirect correlations for the non-canonical bonded nucleobases. The threshold for the A(N1)-T/U(H3) correlation was increased due to lower signal intensity for that particular coupling. (B) *Pseudomonas aeruginosa* biofilm growth yield at 37°C (5 d) as a function of [K^+], [Na^+] or [Li^+] showing the growth dependence on monovalent cation concentration (K^+>Na^+>Li^+). Error bars indicate standard deviation. (C) Illustration of how structural variability of RNA may allow for the formation of extracellular RNA and DNA networks through hairpins and a mixture of canonical and non-canonical base pairs or tetrads (i.e. Hoogsteen and G-quadruplexes).

bioRxiv preprint doi: https://doi.org/10.1101/527267; this version posted January 22, 2019. The copyright holder for this preprint (which was not certified by peer review) is the author/funder, who has granted bioRxiv a license to display the preprint in perpetuity. It is made available under aCC-BY 4.0 International license.

Supplementary Information for

The biofilm matrix scaffold of *Pseudomonas* species consists of non-canonically base paired extracellular DNA and RNA

Thomas Seviour[1,*], Fernaldo Richtia Winnerdy[2], Wong Lan Li[1], Xiangyan Shi[2], Sudarsan Mugunthan[1], Gurjeet Singh Kohli[1], Heather M Shewan[3], Jason R Stokes[3], Scott A Rice[1,4], Anh Tuân Phan[2], Staffan Kjelleberg[1, 5, 6]

[1]Singapore Centre for Environmental Life Sciences Engineering, Nanyang Technological University, 637551, Singapore. [2]School of Physical and Mathematical Sciences, Nanyang Technological University, 637371, Singapore. [3]School of Chemical Engineering, The University of Queensland, 4072, Brisbane, Australia. [4] The iThree Institute, The University of Technology Sydney, Sydney, 2007, Australia. [5] School of Biological Sciences, Nanyang Technological University, 637551, Singapore. [6] Centre for Marine Bio-Innovation, School of Biological, Earth and Environmental Sciences, University of New South Wales, Sydney, 2052, Australia.

Correspondence to: twseviour@ntu.edu.sg

This PDF file includes:

Supplementary Figs. 1 to 19
Supplementary Tables 1-2

bioRxiv preprint doi: https://doi.org/10.1101/527267; this version posted January 22, 2019. The copyright holder for this preprint (which was not certified by peer review) is the author/funder, who has granted bioRxiv a license to display the preprint in perpetuity. It is made available under aCC-BY 4.0 International license.

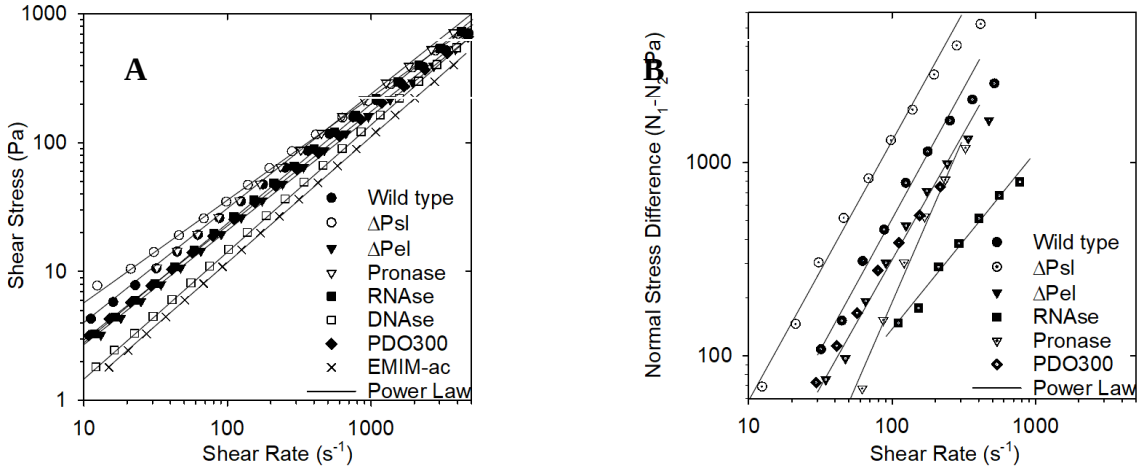

Supplementary Fig. 1: (A) Shear stress and (B) normal stress differences ($N_1 - N_2$) as a function of shear rate for *P. aeruginosa* biofilm: wild type; PDO300; ΔPsl, ΔPel; pronase digested; RNase A digested; and DNase I digested wild type biofilm, dissolved in 1-ethyl-3-methylimidazolium acetate (40 mg/mL) at 25 °C, 100 µm rheometer measurement gap, shear stress sweep from 10 to 1000 Pa. ($N_1 - N_2$) is not described for DNase I digested biofilm as its normal force (F_N) is less than the resolution of the rheometer (i.e. 0.1 N) and is set to zero for calculating ($N_1 - N_2$). Lines indicate power-law fits to the data. The power law dependences of shear stress on shear rate (m) (see Table S1) indicate Newtonian-like rheological properties**.**

bioRxiv preprint doi: https://doi.org/10.1101/527267; this version posted January 22, 2019. The copyright holder for this preprint (which was not certified by peer review) is the author/funder, who has granted bioRxiv a license to display the preprint in perpetuity. It is made available under aCC-BY 4.0 International license.

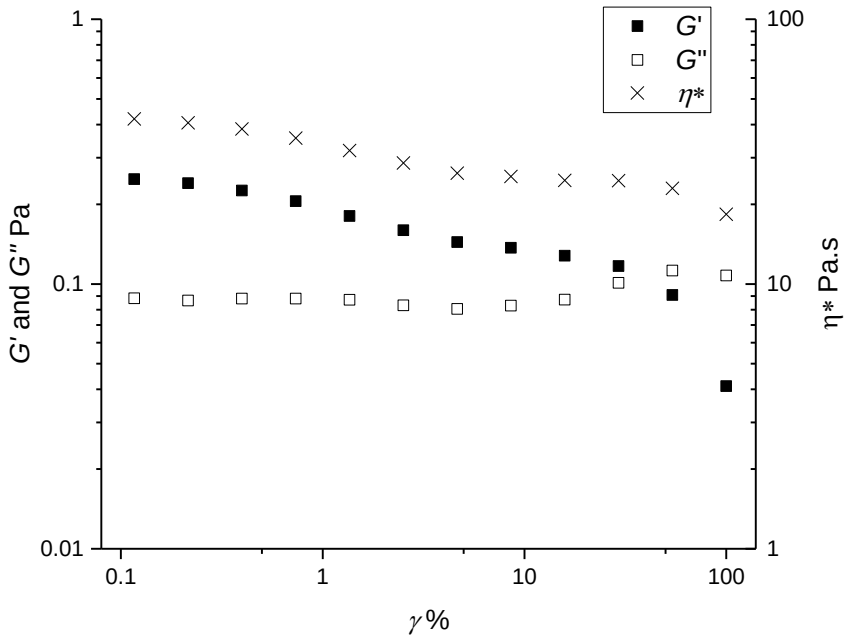

Supplementary Fig. 2: Storage modulus (*G'*), loss modulus (*G''*) and complex viscosity (η*) of *P. aeruginosa* wild type biofilm in amplitude sweep at 25°C, 50 µm gap, 0.1 s^{-1} frequency, showing that the biofilm behaves like a gel at low amplitude (i.e. *G' > G''*). Note, *G'* is not measurable in the DNase I treated biofilm.

bioRxiv preprint doi: https://doi.org/10.1101/527267; this version posted January 22, 2019. The copyright holder for this preprint (which was not certified by peer review) is the author/funder, who has granted bioRxiv a license to display the preprint in perpetuity. It is made available under aCC-BY 4.0 International license.

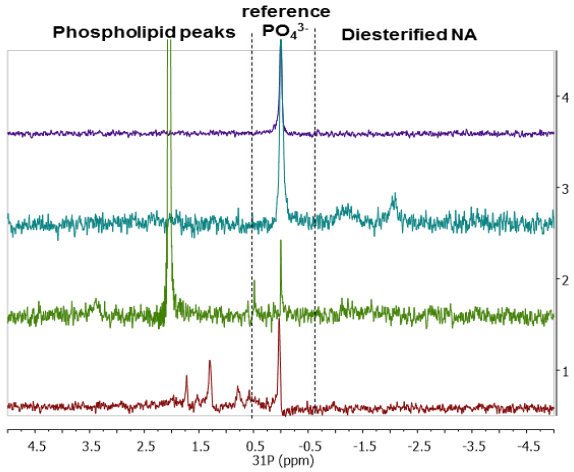

Supplementary Fig. 3: ^{31}P NMR spectrum of H_3PO_4 solution in EMIM-Ac (— upper), lyophilized *P. aeruginosa* wild type biofilm in EMIM-Ac (10 $mg.mL^{-1}$) (— second upper), asolectin standard in EMIM-Ac (— second lower) and SDS and lysozyme-treated *P. aeruginosa* wild type planktonic cells (— lower) at 25°C, showing phospholipid peaks for asolectin in EMIM-Ac, for lysed *P. aeruginosa* cells (SDS, lysozyme) in water, and the absence of phospholipid peaks in the spectrum of *P. aeruginosa* treated with EMIM-Ac.

bioRxiv preprint doi: https://doi.org/10.1101/527267; this version posted January 22, 2019. The copyright holder for this preprint (which was not certified by peer review) is the author/funder, who has granted bioRxiv a license to display the preprint in perpetuity. It is made available under aCC-BY 4.0 International license.

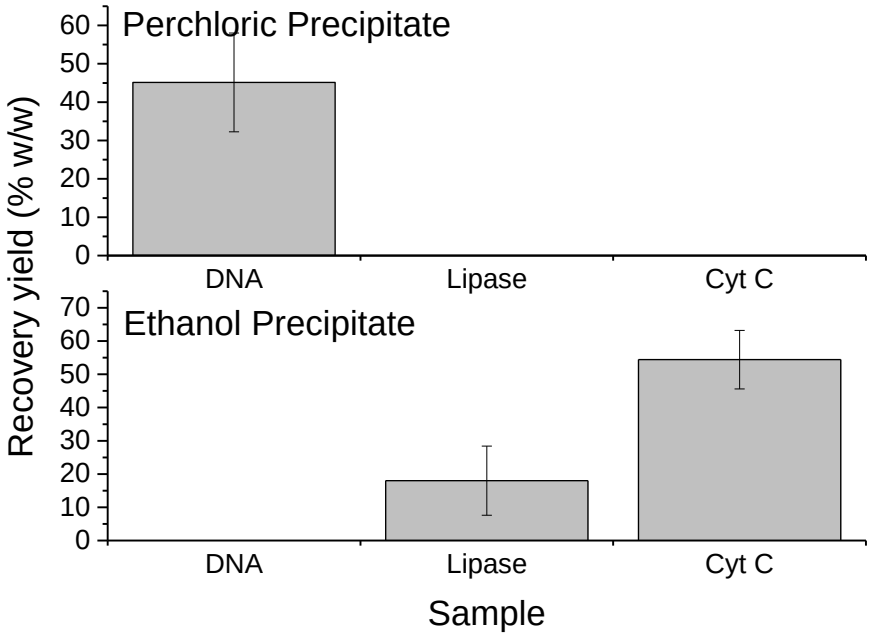

Supplementary Fig. 4: Recovery yield of calf thymus DNA, lipase and cytochrome c standards following EMIM-Ac solubilization and recovery with perchloric acid (upper) followed by ethanol (lower). Error bars indicate standard deviation.

bioRxiv preprint doi: https://doi.org/10.1101/527267; this version posted January 22, 2019. The copyright holder for this preprint (which was not certified by peer review) is the author/funder, who has granted bioRxiv a license to display the preprint in perpetuity. It is made available under aCC-BY 4.0 International license.

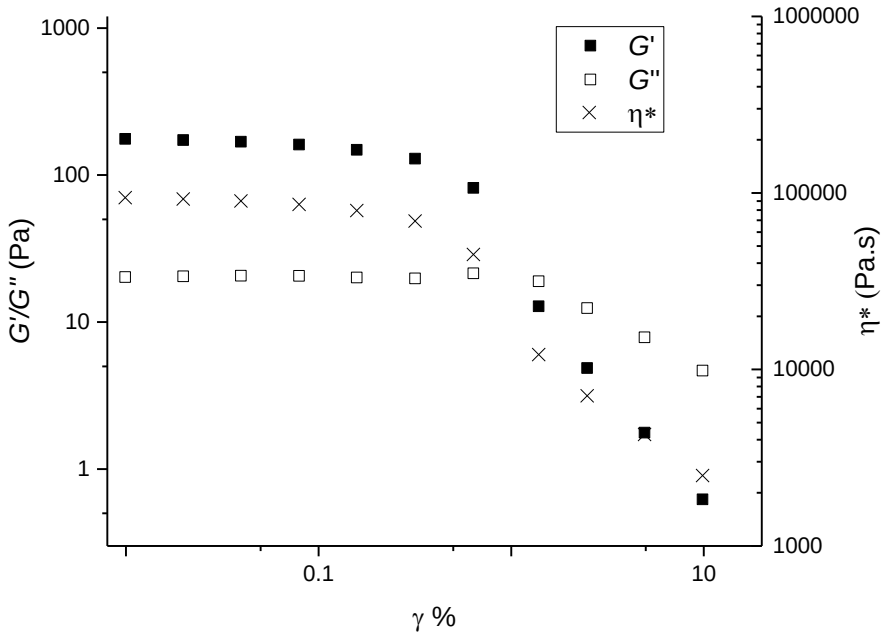

Supplementary Fig. 5: Storage modulus (*G'*), loss modulus (*G''*) and complex viscosity (η*) of *P. aeruginosa* wild type biofilm extracellular nucleic acid gel isolate in amplitude sweep at 25°C, 50 µm gap, 0.1 s^{-1} frequency, showing that the biofilm behaves like a gel at low amplitude (i.e. *G' > G''*).

bioRxiv preprint doi: https://doi.org/10.1101/527267; this version posted January 22, 2019. The copyright holder for this preprint (which was not certified by peer review) is the author/funder, who has granted bioRxiv a license to display the preprint in perpetuity. It is made available under aCC-BY 4.0 International license.

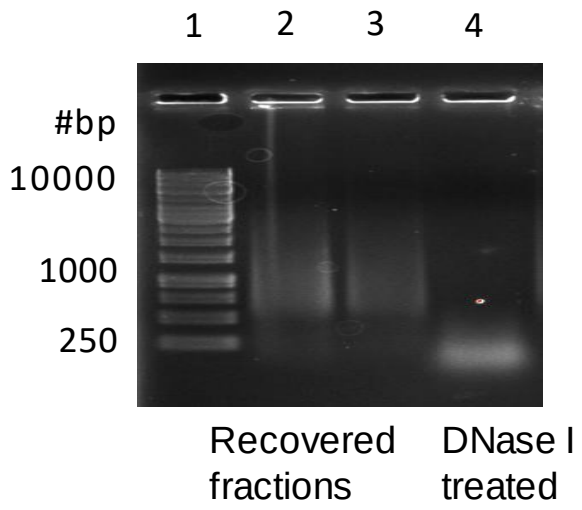

Supplementary Fig. 6: Agarose electrophoretic gel showing *P. aeruginosa* eDNA (Lanes 2 and 3) and digested with DNase (Lane 4). Lane 1 is the GeneRuler 1 kbp ladder.

bioRxiv preprint doi: https://doi.org/10.1101/527267; this version posted January 22, 2019. The copyright holder for this preprint (which was not certified by peer review) is the author/funder, who has granted bioRxiv a license to display the preprint in perpetuity. It is made available under aCC-BY 4.0 International license.

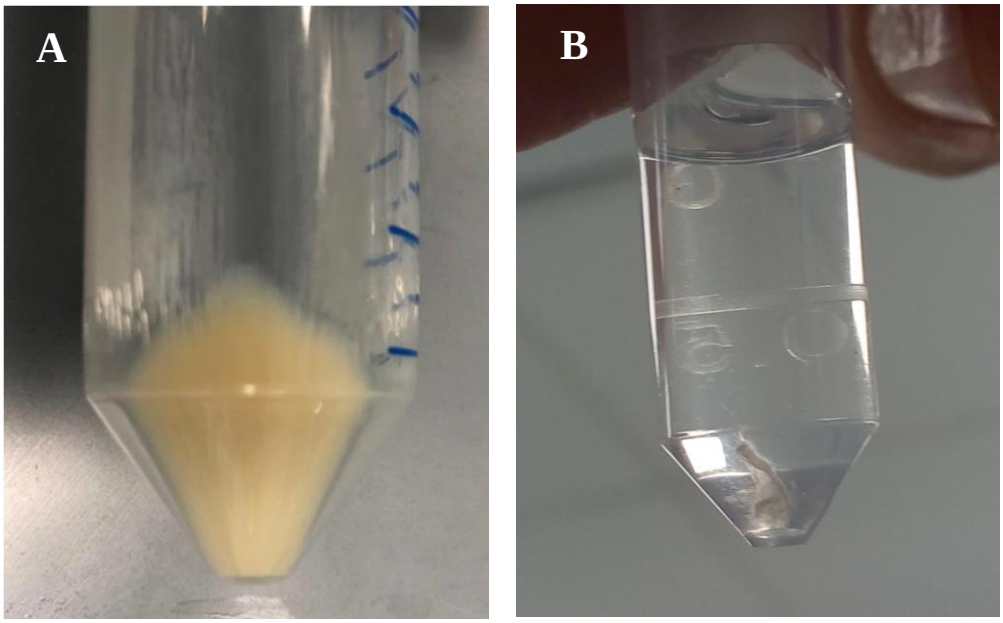

Supplementary Fig. 7: (A) Photograph of *P. aeruginosa* biofilm extracellular polymeric substances recovered by ethanol precipitation (70 % v/v) from 1-ethyl-3-methylimidazolium, dialyzed against double distilled water and then pelleted by centrifugation (10,000 g, 4°C) after it was dissolved (20 $mg.mL^{-1}$) and eDNA first removed by perchloric acid precipitation (5 % v/v), showing that gelation was not observed once the nucleic acids were removed. (B) Photograph of calf thymus DNA recovered from 1-ethyl-3-methylimidazolium after dissolution (6 $mg.mL^{-1}$), perchloric acid precipitation and dialysis against double distilled water showing that gelation is not a universal feature of all DNA following dissolution in 1-ethyl-3-methylimidazolium acetate and perchloric acid precipitation.

bioRxiv preprint doi: https://doi.org/10.1101/527267; this version posted January 22, 2019. The copyright holder for this preprint (which was not certified by peer review) is the author/funder, who has granted bioRxiv a license to display the preprint in perpetuity. It is made available under aCC-BY 4.0 International license.

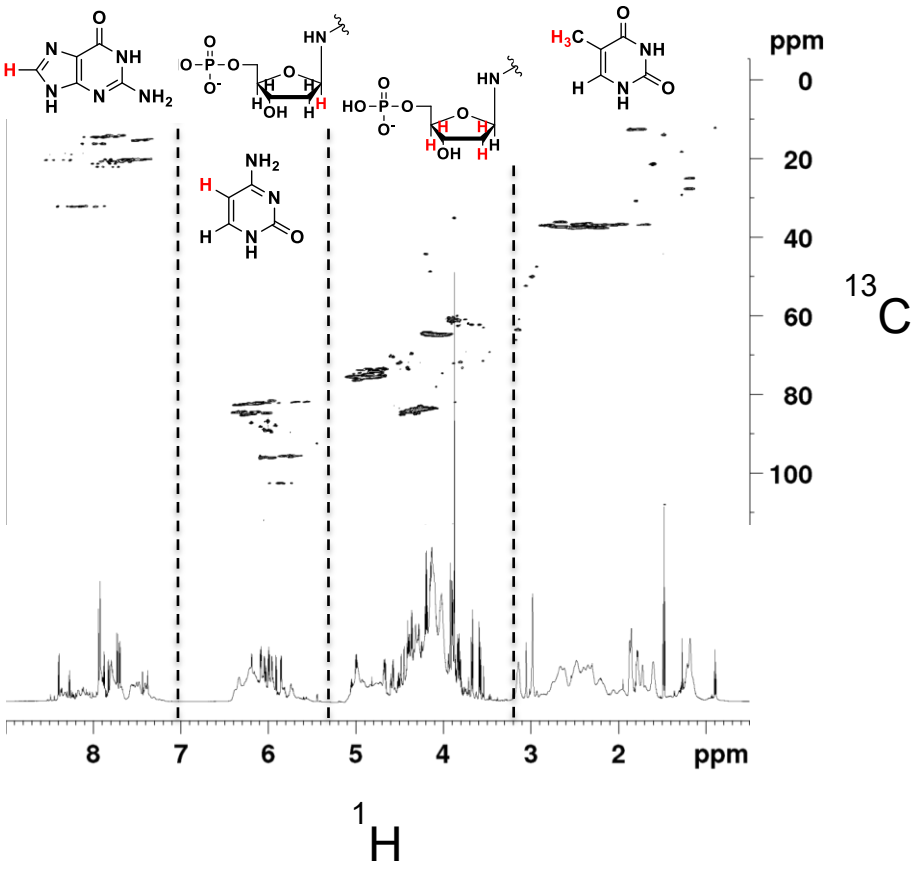

Supplementary Fig. 8 ^{1}H-^{13}C HSQC-TOCSY and 1-D ^{1}H NMR spectra of *P. aeruginosa* biofilm extracellular NA gel isolate following alkalinization (0.1 M NaOD, 10 mg.mL^{-1}, 55°C, 2 h) at 25°C showing a distribution of ^{1}H-^{13}C HSQC-TOCSY cross peaks that is consistent with the presence of nucleic acids and the absence of proteins and hexose-based sugars.

bioRxiv preprint doi: https://doi.org/10.1101/527267; this version posted January 22, 2019. The copyright holder for this preprint (which was not certified by peer review) is the author/funder, who has granted bioRxiv a license to display the preprint in perpetuity. It is made available under aCC-BY 4.0 International license.

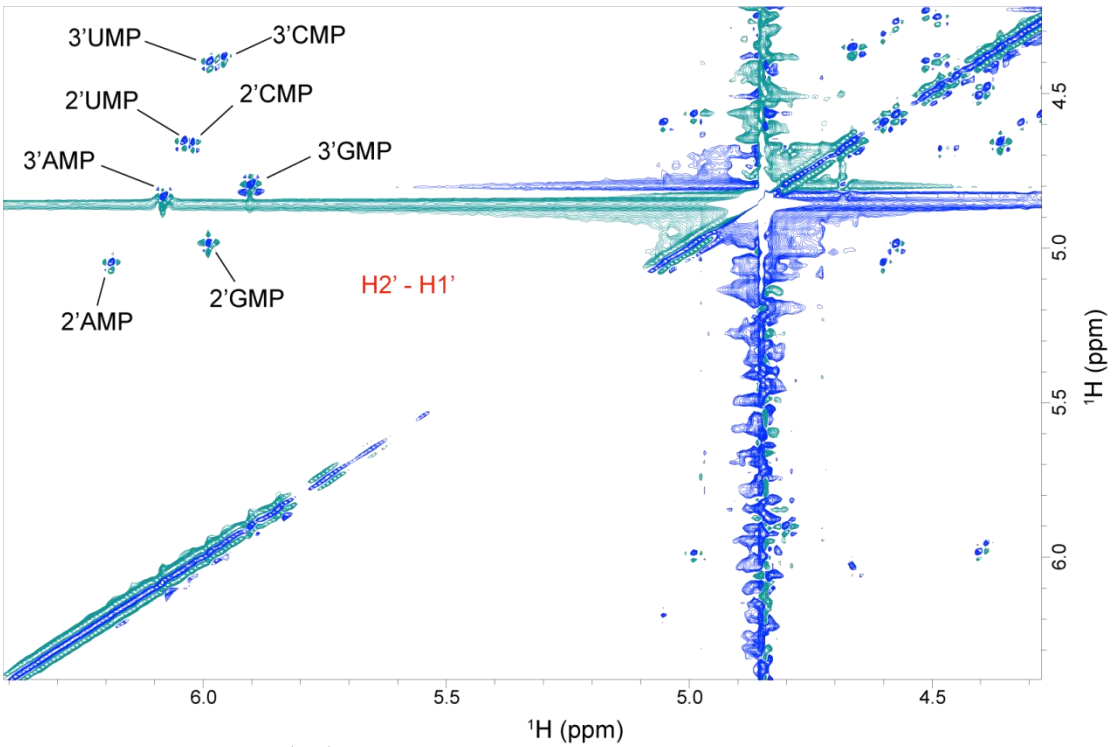

Supplementary Fig. 9: ^{1}H-^{1}H COSY NMR spectrum of *P. aeruginosa* biofilm extracellular NA gel isolate following alkalinization (0.1 M NaOD, 10 mg.mL^{-1}, 55°C, 2 h).

bioRxiv preprint doi: https://doi.org/10.1101/527267; this version posted January 22, 2019. The copyright holder for this preprint (which was not certified by peer review) is the author/funder, who has granted bioRxiv a license to display the preprint in perpetuity. It is made available under aCC-BY 4.0 International license.

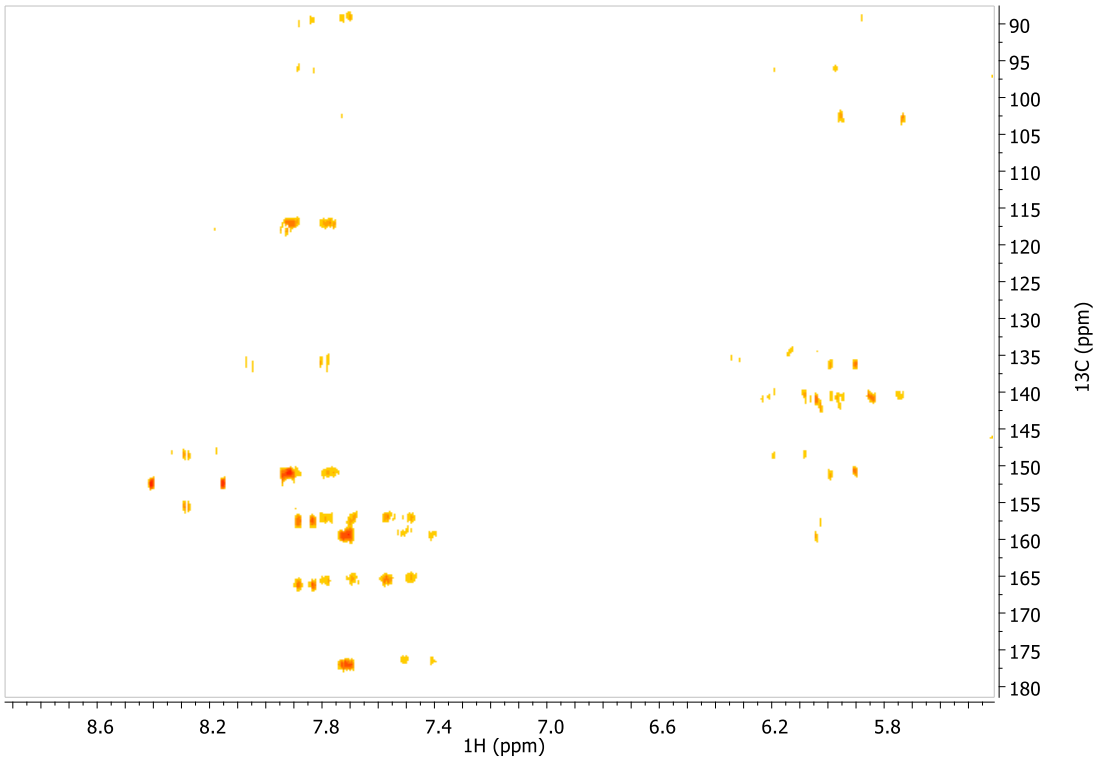

Supplementary Fig. 10: ^{1}H-^{13}C HMBC NMR spectrum of *P. aeruginosa* biofilm extracellular NA gel isolate at 25°C following alkalinization (0.1 M NaOD, 10 mg.mL^{-1}, 55°C, 2 h).

bioRxiv preprint doi: https://doi.org/10.1101/527267; this version posted January 22, 2019. The copyright holder for this preprint (which was not certified by peer review) is the author/funder, who has granted bioRxiv a license to display the preprint in perpetuity. It is made available under aCC-BY 4.0 International license.

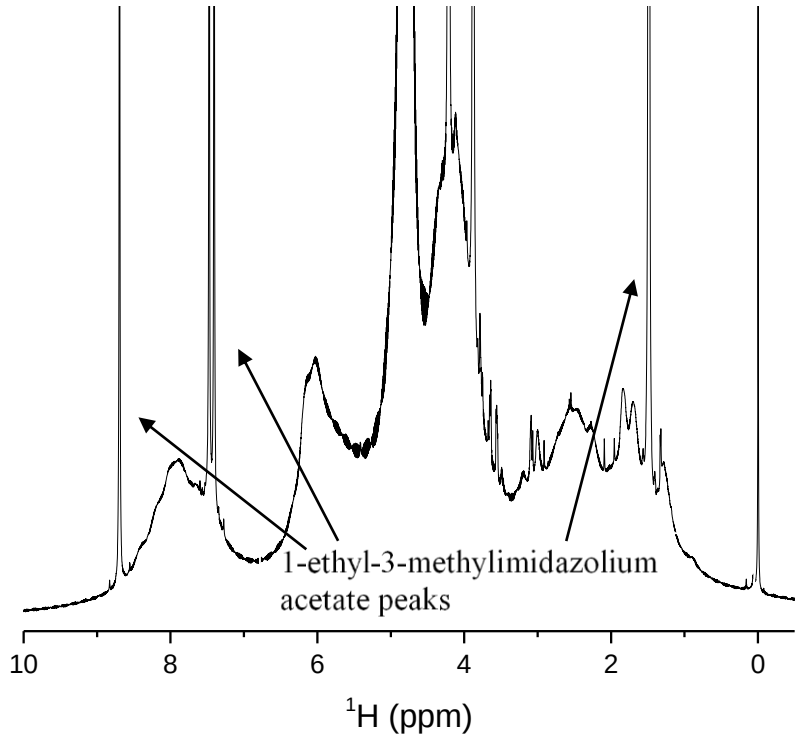

Supplementary Fig. 11: ^{1}H NMR spectra of *P. aeruginosa* biofilm NA gel isolate in D_2O at 25°C.

bioRxiv preprint doi: https://doi.org/10.1101/527267; this version posted January 22, 2019. The copyright holder for this preprint (which was not certified by peer review) is the author/funder, who has granted bioRxiv a license to display the preprint in perpetuity. It is made available under aCC-BY 4.0 International license.

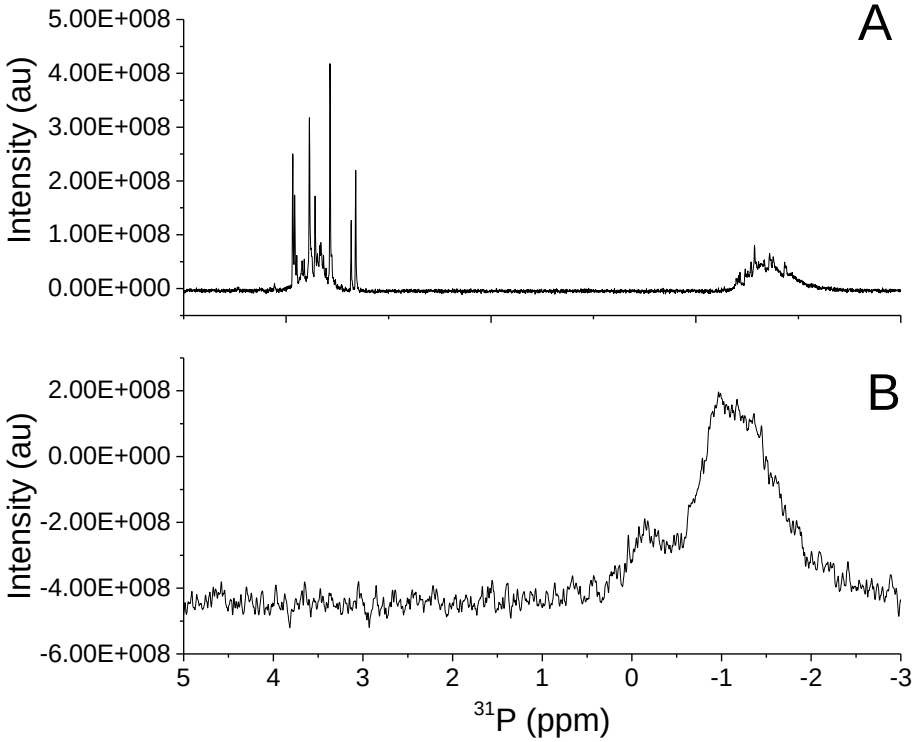

Supplementary Fig. 12: ^{31}P NMR spectrum of RNA standard (torula yeast) at 25°C following alkalinization (0.1 M NaOD, 10 mg.mL^{-1}, 55°C, 2 h) (A) and in D_2O following EMIM-Ac solubilisation and perchloric acid recovery (10 mg.mL^{-1}) (B) demonstrating that alkalinization only leads to RNA transesterification.

bioRxiv preprint doi: https://doi.org/10.1101/527267; this version posted January 22, 2019. The copyright holder for this preprint (which was not certified by peer review) is the author/funder, who has granted bioRxiv a license to display the preprint in perpetuity. It is made available under aCC-BY 4.0 International license.

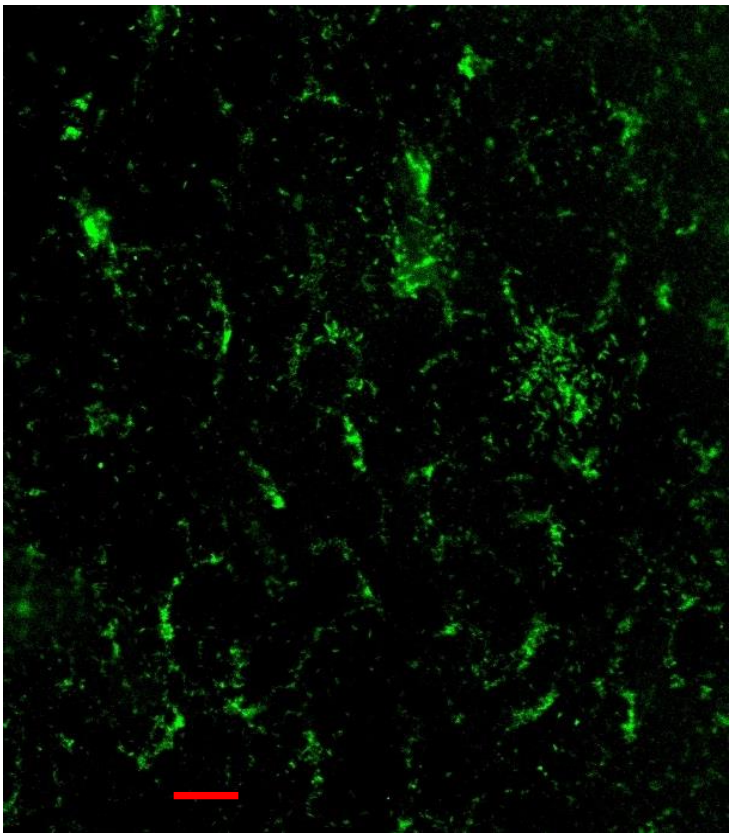

Supplementary Fig. 13: Micrograph of *P. aeruginosa* NA gel isolate, digested with DNase I and stained green with SYTO RNASelect, showing that SYTO RNASelect is binding to extracellular RNA (scale bar 10 µm).

bioRxiv preprint doi: https://doi.org/10.1101/527267; this version posted January 22, 2019. The copyright holder for this preprint (which was not certified by peer review) is the author/funder, who has granted bioRxiv a license to display the preprint in perpetuity. It is made available under aCC-BY 4.0 International license.

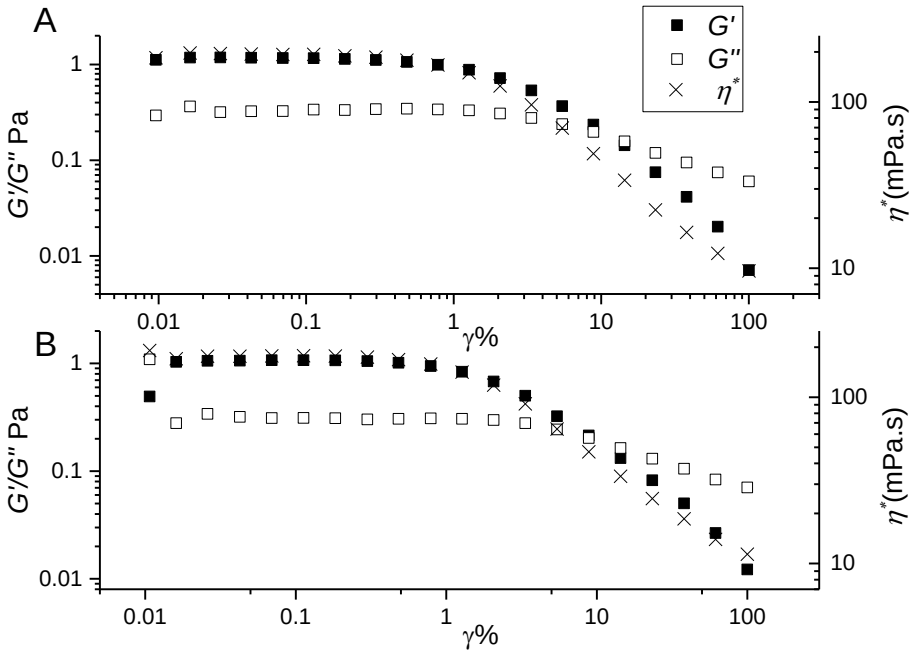

Supplementary Fig. 14: Storage modulus (*G'*), loss modulus (*G''*) and complex viscosity (η*) of *P. aeruginosa* wild type biofilm extracellular nucleic acid gel isolate in amplitude sweep at 25°C, 50 µm gap, 0.1 s^{-1} frequency, showing that the biofilm behaves like a gel at low amplitude (i.e. *G' > G''*) even after digestion with RNase III (A) and RNase H (B).

bioRxiv preprint doi: https://doi.org/10.1101/527267; this version posted January 22, 2019. The copyright holder for this preprint (which was not certified by peer review) is the author/funder, who has granted bioRxiv a license to display the preprint in perpetuity. It is made available under aCC-BY 4.0 International license.

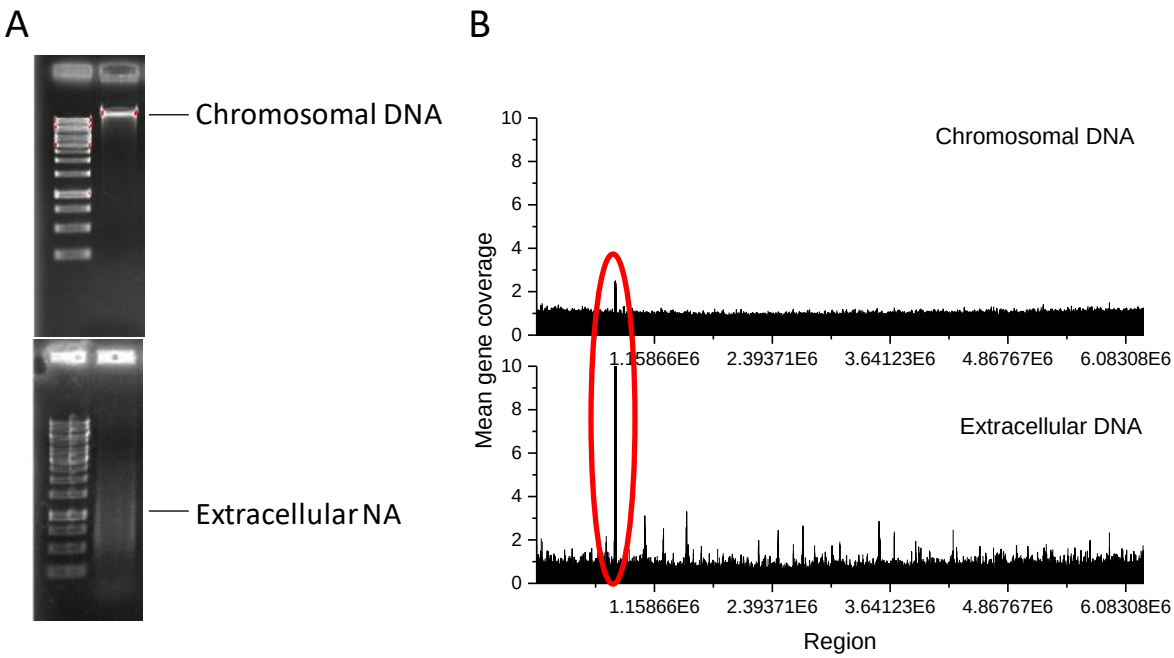

Supplementary Fig. 15: Agarose gel loaded with chromosomal DNA extracted from *P. aeruginosa* pre-culture planktonic cells (upper) and extracellular NA gel isolate (lower) (A). Gene coverage of *P. aeruginosa* biofilm chromosomal (upper) and extracellular (lower) DNA normalized against *rpoB* numbers. The red oval denotes the peak resulting from bacteriophage Pf1 genes (B).

bioRxiv preprint doi: https://doi.org/10.1101/527267; this version posted January 22, 2019. The copyright holder for this preprint (which was not certified by peer review) is the author/funder, who has granted bioRxiv a license to display the preprint in perpetuity. It is made available under aCC-BY 4.0 International license.

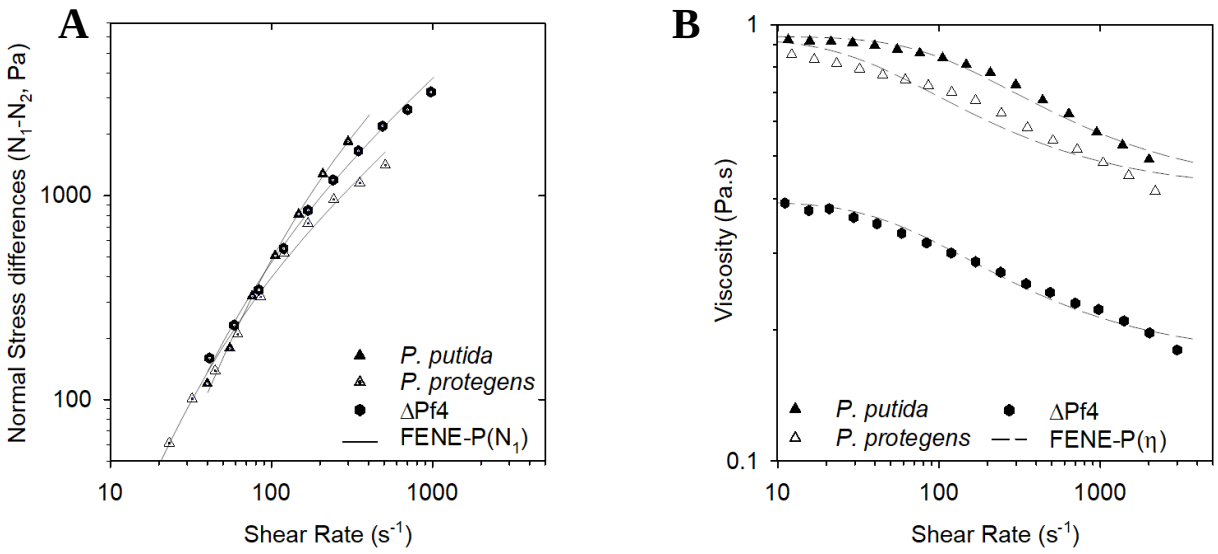

Supplementary Fig. 16: (A) Normal stress differences ($N_1 - N_2$) and (B) shear stress as a function of shear rate for *Pseudomonas* biofilms: *P. putida*, *P. protogens* and *P. aeruginosa* ΔPf4, dissolved in 1-ethyl-3-methylimidazolium acetate (40 mg.mL^{-1}) at 25 °C. Lines indicate FENE-P fits to the data.

bioRxiv preprint doi: https://doi.org/10.1101/527267; this version posted January 22, 2019. The copyright holder for this preprint (which was not certified by peer review) is the author/funder, who has granted bioRxiv a license to display the preprint in perpetuity. It is made available under aCC-BY 4.0 International license.

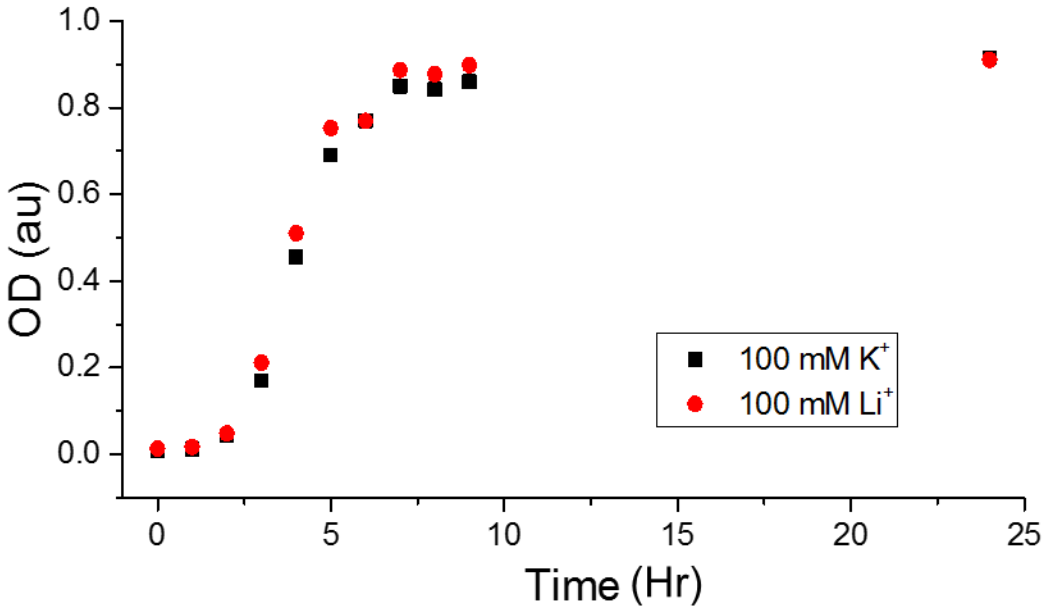

Supplementary Fig. 17: Overnight growth curve for *P. aeruginosa* cells grown in lithium and potassium enhanced modified M9 media, showing that potassium does not enhance planktonic growth over lithium.

bioRxiv preprint doi: https://doi.org/10.1101/527267; this version posted January 22, 2019. The copyright holder for this preprint (which was not certified by peer review) is the author/funder, who has granted bioRxiv a license to display the preprint in perpetuity. It is made available under aCC-BY 4.0 International license.

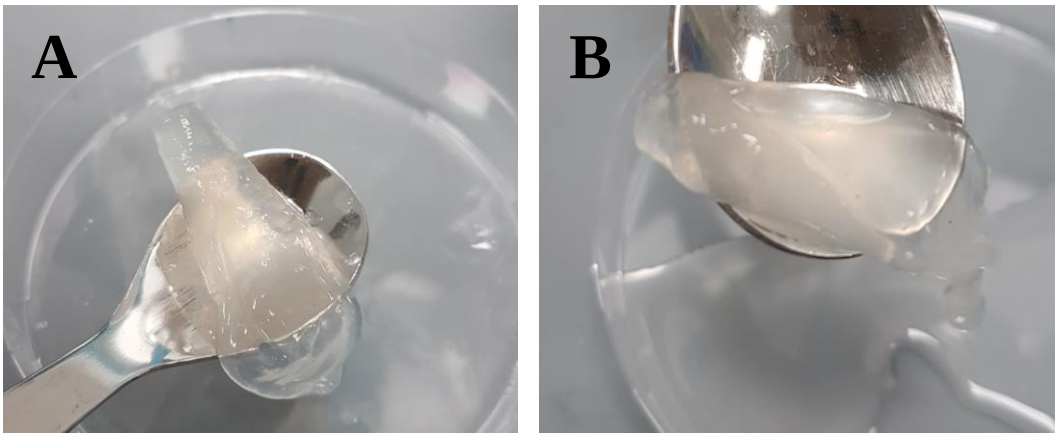

Supplementary Fig. 18: Photograph of nucleic acid gel extracted from (A) *P. protegens* and (B) *P. putida*.

bioRxiv preprint doi: https://doi.org/10.1101/527267; this version posted January 22, 2019. The copyright holder for this preprint (which was not certified by peer review) is the author/funder, who has granted bioRxiv a license to display the preprint in perpetuity. It is made available under aCC-BY 4.0 International license.

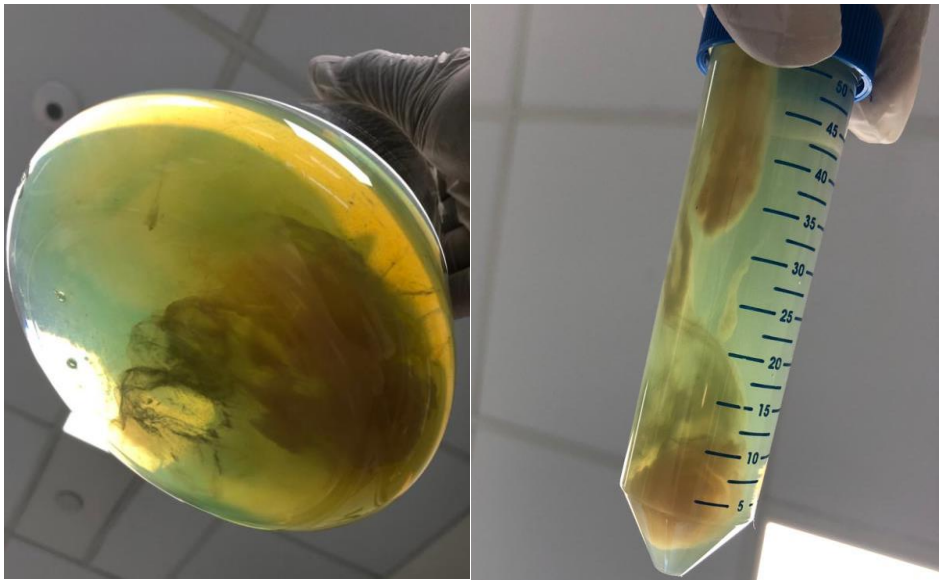

Supplementary Fig. 19: Photographs of *P. aeruginosa* biofilm after 5-d static growth in lysogeny broth medium at 37°C in 2 L Erlenmeyer flask (A) before centrifugation and (B) in 50 mL centrifuge tube after centrifugation showing the separation of biofilm from supernatant.

bioRxiv preprint doi: https://doi.org/10.1101/527267; this version posted January 22, 2019. The copyright holder for this preprint (which was not certified by peer review) is the author/funder, who has granted bioRxiv a license to display the preprint in perpetuity. It is made available under aCC-BY 4.0 International license.

Supplementary Table 1: Power law exponent (i.e. n in $N_1 = K\dot{\gamma}^n$ and m in $\sigma = K_\sigma\dot{\gamma}^m$) of *P. aeruginosa* biofilms following dissolution in EMIM-Ac. m values approaching unity indicate a Newtonian-like fluid property. Viscosity is slightly shear thinning (m = 0.8 to 0.9) for all samples except RNase, DNase and EMIM-Ac which are Newtonian like ($m \geq 0.93$), which would be expected from dilute polymer solutions in viscous fluids (i.e. Boger fluids).

	$\sigma = K_\sigma\dot{\gamma}^m$				$N_1 = K_{N1}\dot{\gamma}^n$			
Sample	**K_σ**		***m***		**K_{N1}**		***n***	
	Ave.	**Std Dev**	**Ave.**	**Std Dev**	**Ave.**	**Std Dev**	**Ave.**	**Std Dev**
P. aeruginosa wild type	0.63	0.08	0.84	0.01	1.44	0.45	1.36	0
ΔPsl	1.26	0.35	0.76	0.04	7.81	5.18	1.21	0.15
ΔPel	0.35	0	0.89	0	0.58	0.15	1.34	0.02
Pronase	0.55	0.03	0.89	0	0.18	0.11	1.64	0.08
RNase	0.34	0.01	0.93	0	2.11	0.09	0.91	0.01
P. putida	1.32	0.01	0.91	0.01	0.56	0.16	1.48	0.08
PDO300	0.73	0.35	0.89	0.01	2.33	0.59	1.10	0.03
P. protegens	1.14	0.01	0.90	0.01	2.75	1.30	1.10	0.11
ΔPf4	0.57	0.02	0.87	0.01	1.59	1.25	1.33	0.24
DNase	0.20	0.01	0.99	0.01	-		-	
EMIM-Ac	0.13	0	0.98	0	-		-	

Supplementary Table 2: Fitting parameters for the FENE-P model including λ_1 = relaxation time, b = a measure of the relative extensibility of the model spring, η_s = solvent viscosity, η_p = polymer contribution to the viscosity. Molecular extensibility and relaxation times, as predicted by FENE-P, decrease in accordance with elasticity.

	Average					**Std. Deviation**			
Sample	b	λ_1	η_p	η_s		b	λ_1	η_p	η_s
P. aeruginosa wild type	2248.5	0.322	0.260	0.145		643.1	0.066	0.040	0.0026
ΔPsl	3511.5	0.676	0.381	0.161		1000.9	0.219	0.113	0.0114
ΔPel	2000.8	0.227	0.110	0.133		637.8	0.056	0.000	0.0025
Pronase	1871.8	0.103	0.197	0.167		693.1	0.047	0.015	0.0339
RNase	399.2	0.102	0.095	0.183		17.6	0.008	0.003	0.0077
PDO300	909.4	0.453	0.138	0.147		134.2	0.023	0.026	0.0007
DNase	135.7	0.005	0.020	0.129		106.8	0.001	0.011	0.0112
ΔPf4	865.4	0.230	0.243	0.166		129.9	0.034	0.022	0.0072
P. protegens	137.2	0.175	0.501	0.414		19.2	0.028	0.025	0.0013
P. putida	336.9	0.071	0.544	0.440		53.5	0.002	0.018	0.0199